energies

MDPI

Review

Stray Losses in Structural Components of Power Transformers

Stipe Mikulić [1] **and Damir Žarko** [2,*]

[1] KONČAR—Distribution and Special Transformers Inc., Josipa Mokrovića 8, 10090 Zagreb, Croatia; stipe.mikulic@koncar.hr
[2] Faculty of Electrical Engineering and Computing, University of Zagreb, Unska 3, 10000 Zagreb, Croatia
* Correspondence: damir.zarko@fer.unizg.hr

Abstract

The paper provides a comprehensive overview of stray losses in conductive structural parts of power transformers, addressing the effects of stray magnetic fields on simple conductive plates, the distribution of additional losses across structural components and measures for their reduction. It examines the (im)possibility of directly measuring stray losses and presents methods for their indirect measurement, highlighting the generation of fault gases due to thermal faults and the importance of understanding multiphysical (electromagnetic–thermal) coupling in calculating stray losses. A problem rarely mentioned in the literature but confirmed here by measurements, is the excessive heating of the connecting elements of the clamping system caused by circulating currents.

Keywords: transformer; stray magnetic field; stray losses; eddy currents; structural components; tank; cover; clamping structures; thermal fault; electromagnetic–thermal coupling; circulating currents

1. Introduction

Stray losses in power transformers make up a smaller portion of the total load losses and are almost impossible to measure directly [1]. Therefore, accurate calculation methods and measures for their reduction provide a distinct advantage in the highly competitive transformer industry [2]. A specific category of stray losses occurs in the conductive structural components of the transformer (such as the tank, cover and clamping structures). The primary function of these components is mechanical and they are not intended to carry current. However, the presence of a stray magnetic field induces eddy currents within them, resulting in additional losses.

If stray losses account for approximately 15% of a transformer's load losses, then as a rough approximation, losses in the conductive structural elements of the transformer constitute about one-third of the stray losses [3], which is roughly 5% of the transformer's total load losses. These additional losses in the structural elements are not negligible and are actively minimised, as they represent a measurable energy cost that is valued through the capitalisation of losses (primary stray losses). There are also localised losses in structural elements (secondary stray losses) that are not significant in magnitude, but they can create areas of high local temperature (hot-spots) that thermally degrade insulation, lead to the generation of fault gases, and affect transformer reliability.

The implementation of measures to reduce stray losses in structural parts does not necessarily eliminate critical hot-spot areas [4]. Measures that reduce total stray losses generally involve increased material usage, reduced electrical and magnetic clearances, greater design complexity, and similar factors, all of which contribute to an overall increase

Check for updates

Academic Editor: Sérgio Cruz

Received: 8 November 2025
Revised: 12 December 2025
Accepted: 22 December 2025
Published: 8 January 2026

Copyright: © 2026 by the authors. Licensee MDPI, Basel, Switzerland. This article is an open access article distributed under the terms and conditions of the Creative Commons Attribution (CC BY) license.

in transformer cost [5]. Consequently, the design of a power transformer represents a compromise between cost and performance [6]. Unlike reducing the capitalised losses of the transformer, applying precise measures to eliminate critical hot-spot areas directly affects transformer reliability. From the perspective of the power system, this criterion is more significant than the loss criterion.

In the transformer manufacturing process, certain aspects are not fully covered by standard factory tests. The temperature-rise test is typically performed at the extreme minus tap position, which produces the highest load losses, while stray losses in structural components are generally highest at the extreme plus tap position, corresponding to the highest short-circuit voltage. As a result, there are borderline cases where the effects of local overheating caused by the stray magnetic field may be marginally acceptable at the minus tap position but critical at the plus tap position.

In addition to the aforementioned, there are areas of stray losses that cause localised overheating of structural components which are less studied in the literature. One such area involves circulating currents in the connecting elements of the clamping structures. Although this is a marginal issue, from a reliability perspective it remains an important factor in understanding the complete mechanism of stray loss generation.

This paper presents an overview of published knowledge and practices concerning stray losses in conductive structural components of power transformers. It discusses their basic origin, categorisation by component with known reduction measures, general dependence on transformer ratings, load, temperature, and frequency according to the law of similarity, and methods for direct and indirect measurement.

2. Stray Magnetic Field and Its Effects

All stray losses in a transformer, whether within or outside the windings, originate from the stray magnetic field. The term "stray" is appropriate as it denotes the portion of magnetic energy that can no longer be effectively utilised for transformation but instead causes additional losses within the transformer or dissipates into the surrounding space. There are two main sources of the stray magnetic field in a transformer [7]:

- the leakage field from the windings, i.e., the flux that does not simultaneously link the low-voltage and high-voltage windings (with the short-circuit voltage u_k, or more precisely its reactive component u_σ, being a measure of the leakage flux where $u_k \approx u_\sigma$), which is largely closed through the structural parts of the transformer,
- the magnetic field from the terminals and connection leads, i.e., current-carrying conductors, which generate a magnetic field in their immediate vicinity (with the current magnitude being a measure of the leakage flux).

The stray magnetic field penetrates conductive structural components not intended to carry current. According to Maxwell's equations and Faraday's law of electromagnetic induction (1) [8], an eddy electric field and, consequently, a time-varying voltage are generated within these components, inducing eddy currents whose magnetic field opposes the source field. The interaction between the induced eddy currents and the incident magnetic field within the material results in power dissipation and energy loss as heat.

$$\nabla \times \boldsymbol{E} = -\frac{\partial \boldsymbol{B}}{\partial t}, \quad \boldsymbol{J}_e = \sigma \cdot \boldsymbol{E} \tag{1}$$

2.1. Penetration Depth, Excitation Type and Material Properties

The mechanism of eddy current generation depends on the material properties, the geometry of the element and the orientation of the alternating magnetic field relative to

the component surface. The parameter δ, with the dimension of length, is defined as the penetration depth according to [8]

$$\delta = \sqrt{\frac{2}{\omega \mu \sigma}} \tag{2}$$

where ω is the angular frequency of the excitation field, μ is the magnetic permeability of the material and σ is the electrical conductivity of the material. The ratio of the element thickness to the penetration depth ($2b/\delta$) is the dominant factor in the distribution of induced currents within the conductive element [9].

When an alternating electromagnetic field interacts with a conductive material, it is attenuated due to electromagnetic induction. The induced eddy currents within the conductive element (such as a conductor or a plate) generate magnetic fields that oppose the incident field, thereby limiting its penetration. As a result, the induced currents are driven towards the surface, where most of the magnetic field energy and current are concentrated. In electromagnetic theory, this phenomenon is referred to as the skin effect [8,10].

In current-carrying conductors, the skin effect arises from the conductor's own magnetic field. When the redistribution of current is instead caused by the external magnetic field of adjacent conductors, the phenomenon is known as the proximity effect. In winding assemblies, these two effects act cumulatively and are commonly represented by the relative loss increase factor (also referred to as the skin effect coefficient) with respect to the case of direct current (DC) excitation. At the power grid frequency of 50 Hz, the skin effect induced by the conductor's own current is dominant, whereas at higher frequencies (in the kilohertz range), the proximity effect becomes the prevailing mechanism [11,12].

For the structural parts of a transformer (which are not initially current-carrying), the redistribution of induced currents occurs solely due to the external magnetic field. In this case, the sources responsible for the stray losses are located relatively far away (for example, the leakage field from the windings and the tank wall) compared with the small spacing between adjacent conductors in the windings.

In general, an alternating electromagnetic wave is attenuated within a conductive material to approximately 5% of its initial value after penetrating to a depth of about 3δ. The stray losses generated depend on the ratio $2b/\delta$ for the considered element (approximated as a conductive plate) and on the type of surface excitation [8]. Accordingly, two types of surface excitation can be distinguished: tangential and radial (normal) excitation.

2.2. Tangential Magnetic Excitation of a Conductive Plate

In the case of tangential excitation of a conductive plate (Figure 1, Table 1), the electromagnetic field propagates parallel to the plate surface. This configuration simplifies the definition of boundary conditions and allows the problem to be reduced to a one-dimensional calculation through the plate thickness, using Maxwell's equations and classical eddy-current theory [5]. The formula for calculating eddy current losses under tangential excitation (P_{et}) is generally applied to two limiting cases, depending on the ratio between the material thickness and the penetration depth ($2b/\delta$). Accordingly, the losses per unit surface area [W/m^2] are calculated for two types of plates [8]:

Thin plate—the plate thickness is much smaller than the penetration depth $2b << \delta$. The induced eddy currents have no significant influence on the external field that generates them. Instead, eddy currents are restricted by lack of space or high resistivity of the material and are said to be *resistance-limited*.

$$P_{et.thin\ plate} \approx \frac{H^2}{\sigma \delta} \tag{3}$$

where H is the RMS value of the magnetic field strength [A/m].

Thick plate—the plate thickness is much greater than the penetration depth, $2b >> \delta$. The extent of current distribution is limited by the effects of its own field and currents are said to be *inductance-limited*. Beyond a certain thickness, losses reach a steady-state value.

$$P_{et.thick\ plate} \approx \frac{H^2}{\sigma\delta}\frac{1}{6}\left(\frac{2b}{\delta}\right)^3 = \frac{1}{3}\omega^2\sigma\mu^2H^2b^3 \quad (4)$$

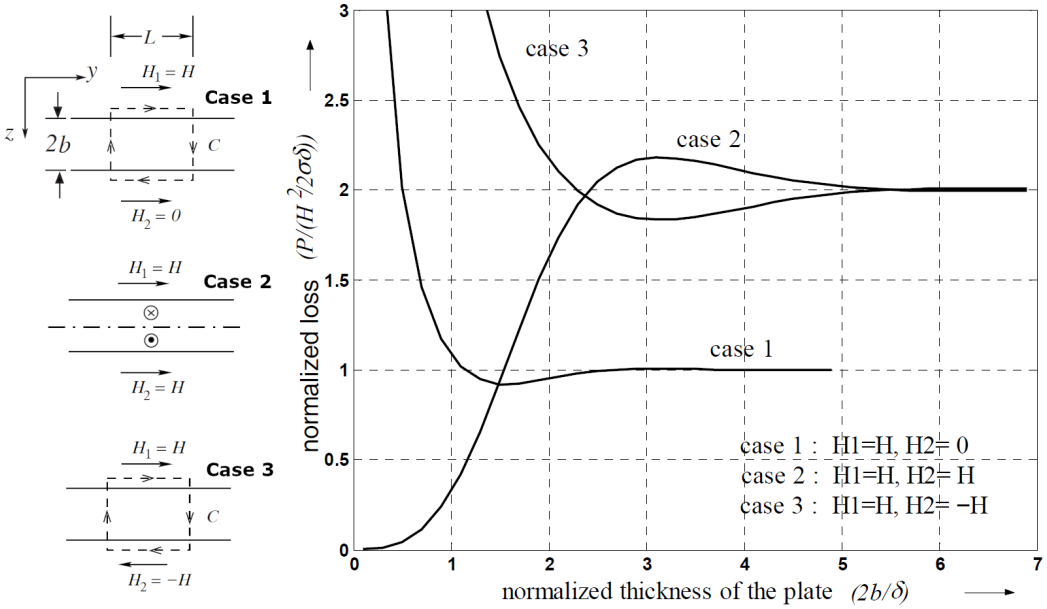


Figure 1. Three types of tangential surface excitation and normalised eddy current losses (H—magnetic field strength; $2b$—plate thickness; δ—penetration depth; σ—electrical conductivity). Source: reproduced with permission from Ref. [5], CRC Press, 2013.

Table 1. Loss distribution for different conductor–plate configurations under tangential excitation. Source: authors.

Case	Configuration	Loss Behavior vs. Plate Thickness
Case 1	Conductor parallel to the conductive plate (e.g., a high-current lead placed near the tank wall)	Losses are very high for a thin plate, while for a thick plate they stabilise after approximately 3δ, becoming independent of plate thickness.
Case 2	Conductor passing through the plate (e.g., a terminal passing through the cover)	Losses increase with plate thickness and stabilise at about 2 p.u. of the normalised value after approximately 5δ, when the conditions become similar to those of two independent plates.
Case 3	Conductive plate placed between two conductors carrying currents in opposite directions	Losses decrease with increasing plate thickness and, for a thick plate, stabilise at approximately 2 p.u. of the normalised value, as in Case 2.

2.3. Radial (Normal) Magnetic Excitation of a Conductive Plate

In the case of radial (normal) excitation of a conductive plate, the magnetic field penetrates the plate perpendicularly and eddy currents are induced on its surface (for example, the leakage field from the windings incident radially with the tank wall). Due to complex boundary conditions, this problem cannot be simplified analytically into a

one-dimensional formulation, as in the case of tangential excitation. Instead, it must be solved in multiple dimensions (2-D or 3-D) using numerical methods [5] (Figure 2).

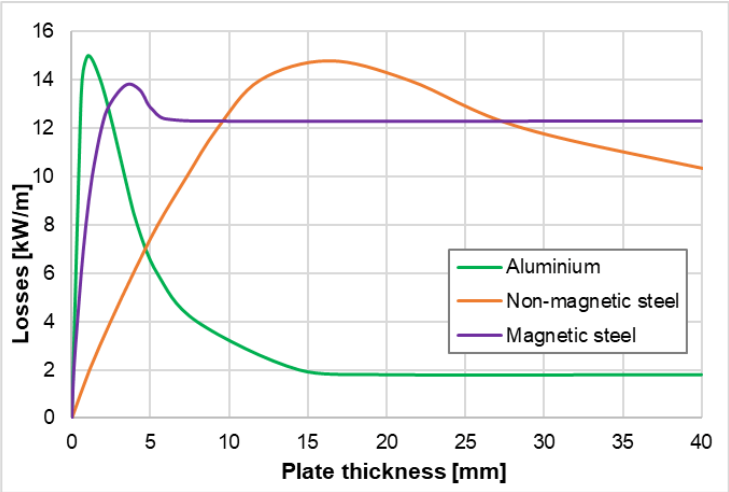


Figure 2. Example of plate losses in different materials under radial surface excitation. Source: authors, adapted from Ref. [5].

In contrast to tangential excitation, there are very few studies in the literature that provide analytical calculations of losses under radial excitation of the plate (P_{er}) [13]. However, Prasad et al. [14] formulated a closed-form expression (5) for calculating the losses in a conductive plate (independent of its thickness) exposed to a normal incident magnetic field and verified the formula using a 3-D finite element method (FEM) numerical analysis

$$P_{er} = lh\left(l^2 + h^2\right)\frac{\omega B_m^2}{96\mu\delta}\frac{\left(1 - e^{-2b/\delta}\right)}{\left|1 + \frac{\mu_0(l+h)}{2\sqrt{2\pi\mu\delta}}\left(1 - e^{-\gamma b}\right)\angle 45^\circ\right|^2} \quad (5)$$

where the magnetic field is incident perpendicularly on the plate along its thickness b, while the other plate dimensions are width l, height h, and eddy-current parameter $\gamma = (1 + j)/\delta$. The presented Formula (5) can be used together with the classical expressions for tangential excitation of the plate, allowing calculation of losses when the incident magnetic field has both tangential and normal components.

In addition to the excitation of the conductive plate itself, the penetration depth of various materials (Table 2) provides guidelines for selecting materials to reduce stray losses. The relationships between material properties and excitation become evident when the loss curves of different materials intersect (thin conductive plates), indicating that the losses in one material exceed those in another. As the plate thickness increases, the losses eventually stabilise, which is characteristic of thick conductive plates.

Table 2. Typical penetration depths of conductive transformer materials at 50 Hz. Source: authors.

Material	μ_r	σ [MS/m]	δ [mm]	$1/\sigma\delta$ [μΩ]
Magnetic structural steel (MS)	300	7.0	1.6	92.0
r Non-magnetic steel (SS)	1	1.4	60.4	11.9
Electrical core lamination steel (ES)	40,000	2.1	0.2	1948.3
Copper (Cu)	1	57.7	9.4	1.8
Aluminium (Al)	1	38.0	11.5	2.3

The primary purpose of structural steel in a transformer is mechanical. Due to mechanical requirements, the typical dimensions of transformer structural components are such that they fall into the category of thick plates ($2b >> \delta$). Eddy current losses in a thick conductive plate are generally proportional to $(1/\sigma\delta)$. Therefore, once the losses have stabilised, the relative losses between structural materials are expected to follow the relation [5]

$$(P_e)_{MS} > (P_e)_{SS} > (P_e)_{Al} > (P_e)_{Cu} \tag{6}$$

given that

$$(1/\sigma\delta)_{MS} > (1/\sigma\delta)_{SS} > (1/\sigma\delta)_{Al} > (1/\sigma\delta)_{Cu}. \tag{7}$$

Among the four structural materials analysed, structural steel exhibits the smallest penetration depth and, due to the high magnetic field intensity, often reaches magnetic saturation (the nonlinear region of the B–H magnetisation curve). Although magnetic saturation is part of the hysteresis phenomenon, its effect is most strongly manifested through the increase in eddy-current losses. When structural steel becomes saturated, its magnetic permeability decreases, which increases the penetration depth. Consequently, higher specific losses are generated deeper within the material. This means that the integral of total losses per unit volume is higher, ultimately resulting in greater eddy-current losses. The increase in eddy-current losses in a thick structural steel plate due to magnetic saturation can be calculated numerically or approximated by applying a linearisation coefficient between 1.3 and 1.5, relative to the losses obtained for the linear unsaturated region, as expressed in (3) and (4) [5].

3. Stray Losses in Conductive Structural Components

When discussing transformer losses, the primary reference is to those losses that generate heat and cause transformer heating. In the general definition of total active power losses (P) in a transformer, these losses are divided into no-load losses (P_0) and load losses (P_t), which are measured during their respective tests, while auxiliary losses (P_{aux}) account for only a minor share of the total losses [15]. Since this paper focuses on stray losses in conductive structural components of transformers, such as the tank, cover and clamping structures (clamping frames, flitch plates, tie bolts, cross plates and other bracing elements), dielectric losses in the insulation are disregarded, as the heat they produce is negligible compared to the losses in current-carrying conductors and the resulting magnetic field effects. Auxiliary losses related to the cooling system supply, i.e., the power losses of pumps and fans, are also neglected.

The load losses P_t consist of two main components: the ohmic losses in the winding resistances $P_{I^2R_{DC}}$ and the stray losses P_{stray}. The stray losses can be further classified by their origin into those occurring within the windings and those outside the windings. The stray losses within the windings include the eddy current losses in the windings $P_{stray.we}$ (resulting from the combined effects of the skin effect and proximity effect) and the circulating current losses between parallel winding conductors $P_{stray.cc}$. The stray losses outside the windings consist of the stray losses in the conductive structural components of the transformer $P_{stray.sc}$ and the stray losses in the core $P_{stray.ce}$ (mainly referring to core edge losses) [5,15,16] (Figure 3).

$$\begin{aligned} P_t &= P_{I^2R_{DC}} + P_{stray} \\ &= P_{I^2R_{DC}} + \underbrace{(P_{stray.we} + P_{stray.cc})}_{\text{stray losses within the winding}} \\ &\quad + \underbrace{(P_{stray.sc} + P_{stray.ce})}_{\text{stray losses outside the winding}} \end{aligned} \tag{8}$$

The classical loss model for soft ferromagnetic materials, which also includes the structural components of transformers, divides losses into two categories: hysteresis losses P_h and classical eddy current losses P_e, generated according to Faraday's law of induction (1). This model is valid when the material properties are considered homogeneous at the macroscopic level, without accounting for the internal microstructure of the material.

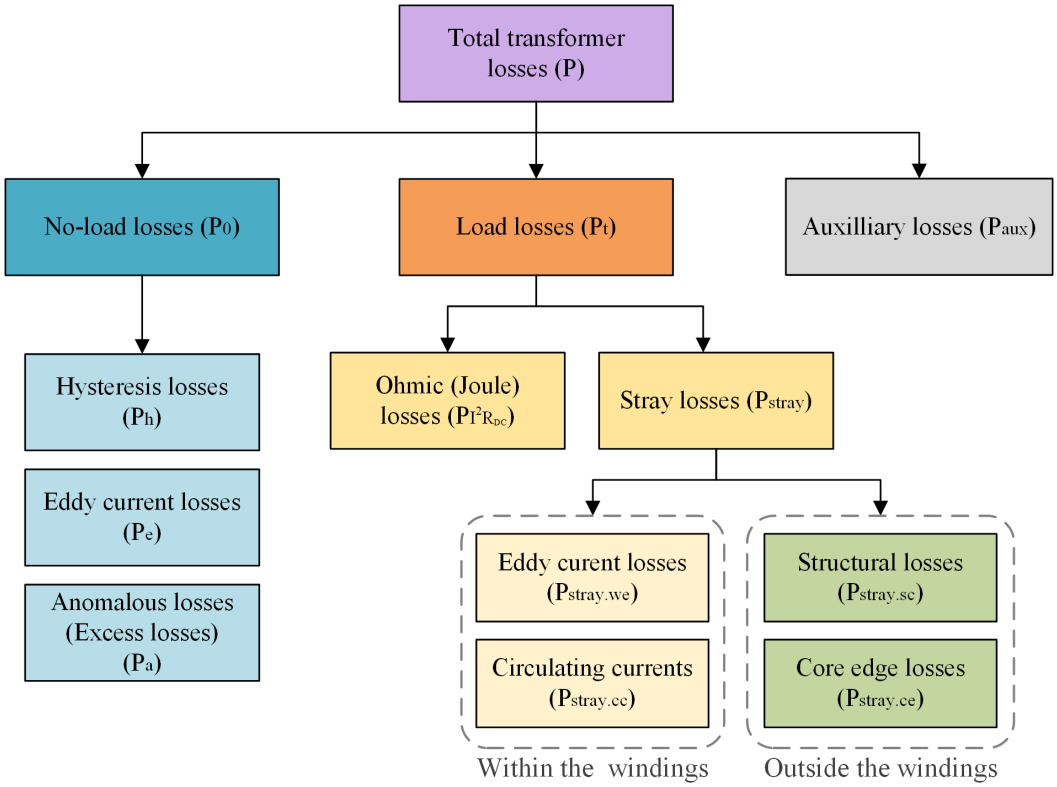


Figure 3. Structure of transformer losses. Source: authors.

When microscopic effects are also considered, it is necessary to account for the movement of discrete magnetisation regions within the material structure, i.e., magnetic domains, which represent the anomalous losses P_a in iron and can even exceed the classical eddy-current losses [17]. Essentially, when analysing stray losses in structural parts, the analysis returns to the relations used for core and no-load losses, as both electrical steel and structural steel are ferromagnetic materials exposed to an alternating magnetic field (electrical steel in the core predominantly to the main flux and structural steel predominantly to the leakage flux).

Apart from relative permeability, electrical conductivity, anisotropy, and other characteristics, the difference between electrical steel and structural steel also lies in the thickness of the material used, specifically in the ratio $2b/\delta$. This results in a different distribution among the three mechanisms of loss generation—hysteresis, classical eddy current, and anomalous losses—in electrical and structural steels [16,17].

$$\begin{aligned} P_{stray.sc} &= P_h + P_e + P_a \\ &= K_h B_m^n f + K_e (B_m f)^2 + K_a (B_m f)^{1.5} \end{aligned} \tag{9}$$

In addition to their dependence on frequency f and the maximum magnetic flux density B_m, in the low-frequency range at which transformers operate and when the material thickness is much greater than the penetration depth $2b >> \delta$, which applies to structural steel, the coefficients K_h, K_e, K_a, and the flux density-dependent exponent n are considered constant [16]. These coefficients are obtained by interpolating the measured

losses in a material exposed to a homogeneous sinusoidal field at different operating points defined by the flux density B_m and frequency f.

In Ref. [16], an example is provided of the determination of the above coefficients and the measurement of the individual loss components (P_h, P_e, and P_a) for various types of steel, including steel grade S235 according to EN 10025-2 [18], which is commonly used as structural steel in transformers.

The conclusion is that for structural steel with a thickness greater than 4 mm and at a frequency of 50 Hz, the effect of magnetic domain movement, i.e., the mechanism of anomalous losses, can be neglected. Most stray losses (at higher flux densities, more than 90%) are due to classical eddy currents, with the remaining part attributed to hysteresis losses. A similar conclusion is stated in Ref. [19], where it is noted that, although structural components are mostly ferromagnetic materials, their hysteresis losses are relatively small compared to eddy-current losses due to their typical dimensions within the transformer.

4. Law of Similarity and the Dependence of Stray Losses on Load, Temperature and Frequency

Stray losses represent a smaller portion of the total load losses P_t in a transformer (in the authors' experience for typical power transformer designs up to 100 MVA, losses P_{stray} account for about 10–20% of P_t), although they increase more rapidly with transformer rated power than the ohmic losses $P_{I^2R_{DC}}$. According to the law of geometric similarity [15], for two transformers made of the same material, with the same specific loading and the same ratio of all linear dimensions X, the stray losses P_{stray} of the similar transformer increase approximately with the fourth to fifth power, X^{4-5}. This increase is faster than the losses $P_{I^2R_{DC}}$ which grow approximately with the third power, X^3, while the cooling surface of the similar transformer increases proportionally with the second power, X^2. In other words, all effects related to stray losses become more pronounced in transformers of higher ratings, which requires additional design measures to reduce them.

An example of the law of similarity and the increase in stray losses is shown in Figure 4, which refers to a transformer with a relatively high short-circuit voltage. The figure presents the nonlinear dependence of the increase in stray losses relative to the ohmic losses $P_{I^2R_{DC}}$. This ratio is highest at the plus tap position, as the energy of the leakage magnetic field is maximal in this position, and consequently, the stray losses are also at their maximum.

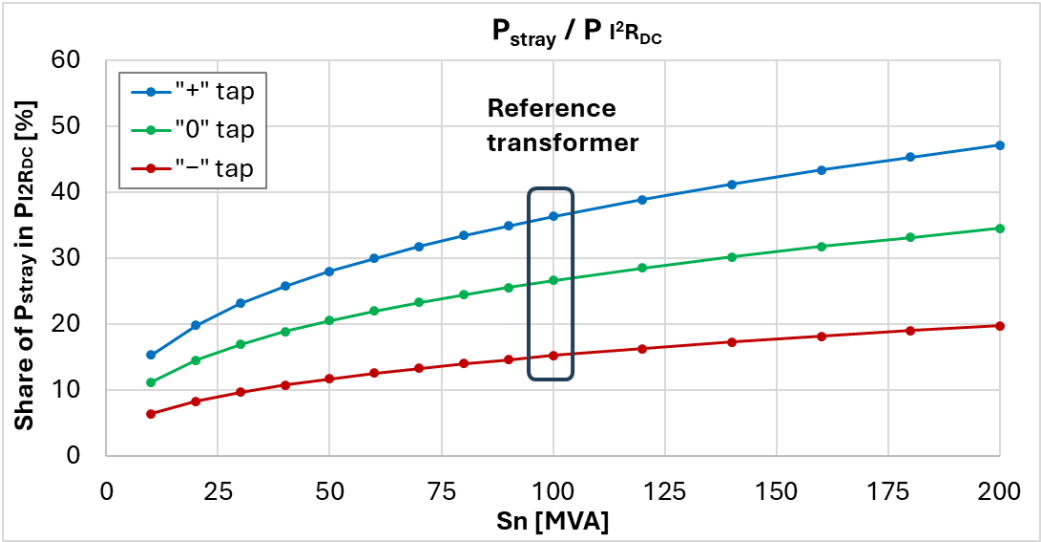


Figure 4. Ratio of transformer losses P_{stray} and $P_{I^2R_{DC}}$ as a function of power for three tap positions (law of similarity on a reference transformer S_n = 100 MVA, u_k = 31–36%). Source: authors.

In general, load losses are expected to be measured at the rated load of the transformer, since the stray losses in structural parts $P_{stray.sc}$ do not increase proportionally to the square of the load current, as do the ohmic winding losses $P_{I^2R_{DC}}$. At lower loads, the leakage magnetic field and consequently the saturation of structural steel are less pronounced, therefore the measures for reducing stray losses do not have their full effect. Moreover, the behavior of stray loss increase also depends on the type of magnetic excitation (tangential or radial), so the losses of a massive steel plate ($2b >> \delta$) subjected to a tangential field follow the law [5].

$$P_{et} \propto I^{1.6-2.0} \times f^{0.5} \times \sigma^{-0.5} \tag{10}$$

where the exponent 1.6 corresponds to the case of a terminal passing through the cover (Case 1, Figure 1), while the exponent 2 refers to the connection lead that is parallel to the material surface (Case 2, Figure 1). In contrast, the losses in a steel plate exposed to a radial magnetic field (tank wall and winding leakage magnetic flux) follow a different law [5].

$$P_{er} \propto I^{2.2-2.5} \times f^{1.9} \times \sigma^{0.9}. \tag{11}$$

On average, for stray losses in structural components $P_{stray.sc}$ where loss reduction measures have been applied, their general dependence on the load current is quadratic, with the current exponent increasing beyond 2 under overload conditions.

The dependence of stray losses on resistivity ρ, i.e., on the electrical conductivity σ of the material, is approximately the same for both the windings and the tank, which in most transformers account for the largest portion of stray losses and can be expressed as [5].

$$P_{stray} \propto \frac{1}{\rho} \quad or \quad P_{stray} \propto \sigma. \tag{12}$$

Since metals have a positive temperature coefficient of resistance, an increase in temperature will lead to a decrease in stray losses P_{stray} [20], unlike ohmic losses $P_{I^2R_{DC}}$, which increase with temperature. This is important when converting losses from the measurement temperature to the reference temperature of 75 °C, at which transformer losses are usually guaranteed.

Regarding frequency dependence, stray losses due to eddy currents in the windings $P_{stray.we}$ exhibit a quadratic dependence, with the exponent decreasing as frequency increases. In structural components $P_{stray.sc}$, the dependence is determined by the type of excitation. For radial excitation, the frequency dependence is slightly less than quadratic, while for tangential excitation the exponent is 0.5. Due to the different exponents, the total structural stray losses $P_{stray.sc}$ depend on frequency according to the ratio of radial and tangential excitation components, which ultimately results in an approximately linear dependence [5], whereas the standard [21] specifies an exponent value of 0.8.

$$P_{stray.we} \propto f^2 \quad and \quad P_{stray.sc} \propto f^{0.8-1.0} \tag{13}$$

5. Stray Losses in Structural Components and Measures for Their Reduction

The stray losses of a power transformer and the measures for their reduction are closely related to improving transformer efficiency, as well as to eliminating hot-spot regions, insulation degradation and reduced lifetime. In Refs. [3,22], the distribution of stray losses by components is presented for a 450 MVA single-phase autotransformer, where stray losses P_{stray} account for more than 30% of the total load losses P_t. Within the structure of stray losses, the largest portion corresponds to stray losses due to eddy currents in the windings, followed by the tank and cover, clamping frames, core (with one main

and two return limbs), tank shields and flitch plates. Considering material nonlinearity (B–H characteristic), parts of the transformer where significant saturation occurs exhibit increased losses due to the presence of higher harmonics, as is the case with additional core losses in the outer core packets (Table 3).

Table 3. Structure of stray losses in a 450 MVA single-phase autotransformer. Source: authors, adapted from Ref. [3].

	Linear FEM		Nonlinear FEM *	
Stray Losses	P_t [%]	P_{stray} [%]	P_t [%]	P_{stray} [%]
AC losses in windings	21.8	68.4	21.8	64.8
Tank and cover	3.8	11.8	2.6	7.6
Tank shields	0.5	1.6	1.0	2.9
Clamping plates	2.8	8.8	2.1	6.2
Flitch plates	0.2	0.7	0.2	0.5
Core	2.8	8.7	6.1	18.0
Total	31.8	100.0	33.6	100.0

*—considering saturation up to and including the 9th harmonic.

As previously mentioned, stray losses in structural components are mainly caused by eddy currents. Therefore, measures to reduce them focus on controlling the magnetic flux and induced currents, i.e., reducing stray flux in structural parts and decreasing the magnitude of eddy currents. Reduction can be achieved in several ways, with some of the main guidelines as follows [5,13]:

- use of laminated materials,
- use of materials with high electrical resistivity,
- reduction of magnetic flux by using materials with higher magnetic reluctance (lower permeability),
- redirection of magnetic flux by providing a parallel magnetic path of low reluctance and low losses,
- shielding the incident flux with screens of low permeability and high electrical conductivity,
- cancellation of magnetic flux by counterflow currents, etc.

5.1. Stray Losses in Tank

Of all stray losses in transformer structural components, losses in the tank have been the most extensively studied, as the losses of an unshielded tank constitute the largest portion of $P_{stray.sc}$. This is why research on tank losses began as early as the middle of the last century. Today, it is almost impossible to design large and efficient power transformers without implementing measures to reduce stray losses. Due to mechanical requirements, losses cannot be reduced by decreasing the thickness of structural steel. Instead, specific techniques for redirecting or shielding the magnetic field are applied to the structural steel. The following measures are commonly used to reduce tank losses [4,23–25]:

- magnetic shunts,
- electromagnetic shields,
- increasing the distance between high-current leads and the tank, and
- reducing the distance between the high-current leads themselves.

Magnetic and electromagnetic shielding are also known as passive and active shielding [26]. Although both methods achieve the same effect—shielding the transformer tank with a material that prevents the stray magnetic field from significantly reaching the tank and causing excessive losses—the physical mechanisms by which magnetic field pene-

tration is prevented differ. In magnetic shields, the leakage field is passively redirected, whereas in electromagnetic shields, the incident leakage field is actively counteracted by the field of the induced currents within the shields [4].

It has already been mentioned that the main sources of the stray magnetic field are the windings, the high-current terminals and connection leads. To mitigate the leakage from the windings, single-phase or three-phase magnetic shunts are typically used. Single-phase shunts consists of laminated electrical steel sheets mounted on the inner sides of the tank, except in the area where the tap changer is located. The term single-phase is used because, due to the orientation of the sheets, each shunt primarily captures the leakage field of a single phase. The leakage field of an unshielded tank is greatest along the centre lines of the core limbs (windings) and smaller in the regions between the phases [23].

Since grain-oriented electrical steel (GOES) sheets are more effective for magnetic shunts than non-oriented electrical steel (NOES) sheets [27], the shunts are installed along the axial height of the tank wall so that the rolling direction of the sheets aligns with the direction of the winding leakage flux. In this way, the sheets act as magnetic flux redirectors, diverting the field away from the tank wall and directing it to close through a parallel path of high permeability (low reluctance) and high electrical resistance compared to the structural steel of the tank. When using transformer sheets as magnetic shunts, attention must be paid to the magnitude of the leakage flux to avoid excessive saturation of the shunts and an increase in local losses, as they have a small penetration depth [26].

Tank magnetic shunts are usually arranged with their width parallel to the tank wall (Figure 5), design variant (a) width-wise shunts. A greater reduction in eddy current losses in the tank by single-phase shunts can be achieved by mounting the sheets so that their edge (the sheet thickness typically 0.30 mm or less) is positioned on the face of the tank wall [28], design variant (b) edge-wise shunts. However, this configuration is more difficult to implement across the entire tank and would increase the overall volume of the transformer. For magnetic shielding of high-current leads and the elimination of hot-spot areas on the tank, variant (b) is more effective only when the magnetic field is parallel to the rolling direction of the magnetic shunts [29].

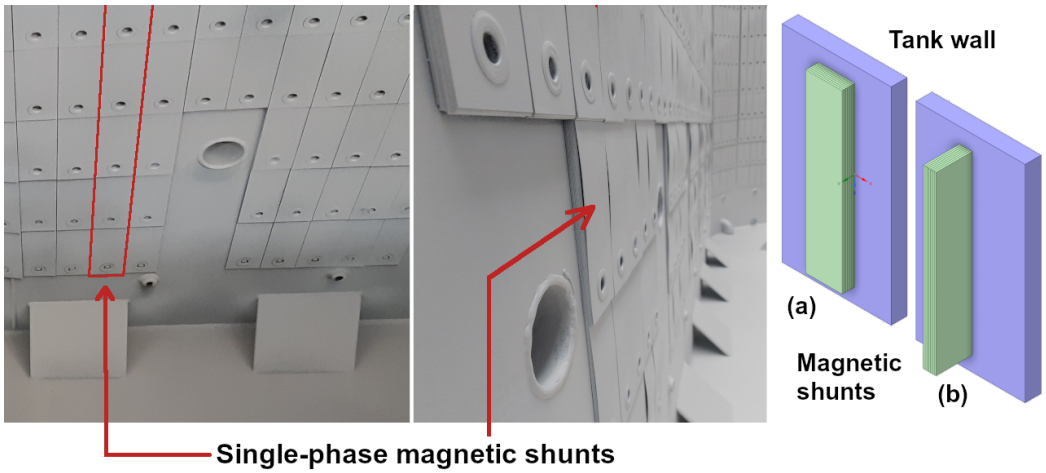


Figure 5. Single-phase magnetic shunts of the transformer tank made of laminated electrical steel, with sheet orientations relative to the tank wall: (**a**) width-wise and (**b**) edge-wise. Source: authors.

The effectiveness of magnetic shielding of the transformer tank depends on the extent to which the tank wall is covered by the shields, with the highest losses occurring on the longer side walls of the tank (HV and LV sides) [30]. In addition, reduced ductility makes the use of laminated sheets as magnetic shunts on irregularly shaped tanks difficult or almost impossible [4,5].

For properly dimensioned shields, the axial height of the shield contributes most to reducing tank losses and for optimal performance, it should extend more than half a metre above the upper and lower levels of the windings [30]. Magnetic shielding of the tank is a highly effective measure, provided that the total losses of the shielded tank and the shields themselves are lower than those of an unshielded tank [4]. Various verified results (calculations confirmed by measurements) indicate a reduction by more than 5 [31], 10 [27] or even 13 times [32], depending on the specific design of each transformer. Shielding also changes the distribution of losses over the surface of the tank wall, with the maximum loss density shifting from the mid-height of the tank (approximately the mid-height of the windings) to the regions corresponding to the upper and lower winding levels.

Unlike single-phase shunts, three-phase magnetic shunts operate on the principle of magnetic flux cancellation (magnetic flux collectors), capturing the leakage fluxes of all three phases, which then cancel each other within the shield itself, $\Phi_{A\sigma} + \Phi_{B\sigma} + \Phi_{C\sigma} \approx 0$ [33]. As a result, they provide a short-circuit path for the three-phase magnetic flux. In this sense, three-phase magnetic shunts protect structural components by cancelling the flux rather than physically redirecting it away from the structural steel, as is the case with single-phase magnetic shunts.

In power transformers, single-phase magnetic shunts are commonly used, although a combination of single-phase shunts (on the shorter side walls) and three-phase shunts (on the longer side walls) can also be applied (Figure 6). This arrangement does not further reduce stray losses in the tank, but it decreases the total mass of shunts required to achieve the same loss reduction effect as single-phase shielding by approximately 25% [34].

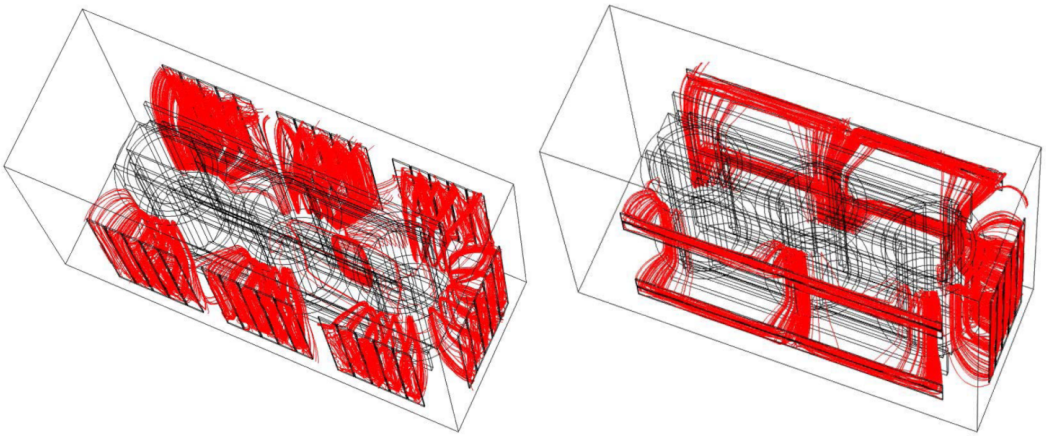


Figure 6. Leakage magnetic flux lines from the windings for single-phase (**left**) and combined single-phase and three-phase magnetic tank shunts (**right**). Source: reproduced with permission from Ref. [34], IEEE, 2017.

In addition to optimising the overall cost of shielding, the use of three-phase magnetic shunts on the transformer tank is also justified when high-current terminals are mounted on the side wall of the tank [35]. Horizontally arranged laminated electrical steel sheets on the tank walls, with the rolling direction of the sheets aligned along the length of the inner tank surface, ensure the capture of the fluxes from all three terminal phases and the resulting field cancellation effect.

Unlike magnetic shunts, which operate by redirecting the magnetic flux, electromagnetic shields use paramagnetic materials with $\mu_r \approx 1$ (most commonly aluminium and copper) that form a magnetic barrier through induced eddy currents [23]. The induced currents in the shields flow in a direction that opposes their source, producing a magnetic field that shields against the incident leakage field. However, this may transfer the incident field to another region of the transformer, where it can cause problems [26]. As a result,

electromagnetic shields lead to a higher concentration of leakage flux in other structural components (e.g., clamping frames) than magnetic shunts, which capture most of the leakage flux. Considering the total stray losses P_{stray}, it is generally accepted that magnetic shunts are more effective than electromagnetic shields [4].

However, the advantage of electromagnetic shields over magnetic shunts lies in their ductility, as they are not as brittle as electrical steel sheets and can therefore be adapted to irregular tank geometries. They can be applied locally near low-voltage, high-current leads positioned close to and parallel with the tank wall to prevent the formation of hot-spot regions and thermal faults [4] (Figure 7). It is therefore essential to properly design their thickness, placement and cooling to ensure that the eddy currents induced within them do not cause excessive losses and turn the shields themselves into sources of hot-spots. To minimise losses, their thickness should be comparable to their penetration depth. In the case of exposure to a magnetic field, the lowest loss value is achieved when the plate thickness is equal to the optimal value reported in Refs. [13,36].

$$2b_{min} = \frac{\pi}{2}\delta \tag{14}$$

which is approximately 15 mm for a Cu plate and 18 mm for an Al plate.

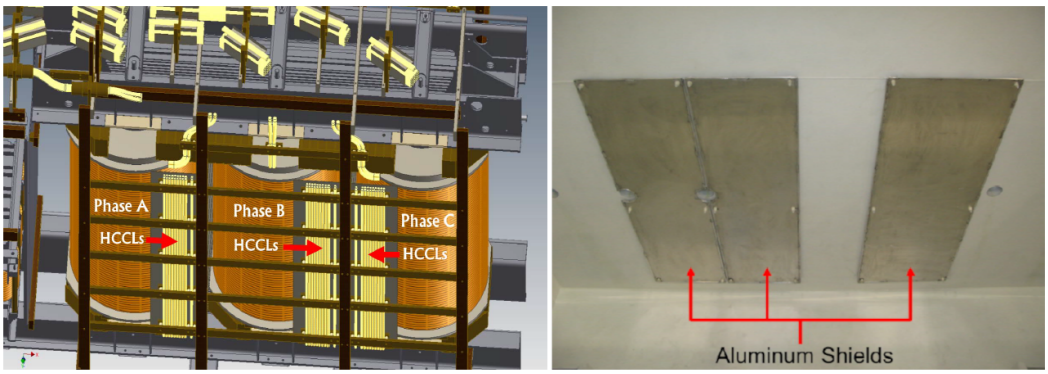


Figure 7. Low-voltage high-current leads and electromagnetic aluminium tank shields. Source: reproduced with permission from Ref. [37], IEEE, 2014.

The tank losses caused by the proximity of high-current leads running parallel to the tank decrease inversely with the distance between the tank and the leads. When electromagnetic shields are applied, the total losses (tank plus shield losses) are lower than those of an unshielded tank and remain approximately constant regardless of the distance between the tank and the leads. The variation with distance is reflected only in the redistribution of losses between the shield and the tank [19]. If aluminium shields are used to protect only the leads of one phase, the local tank losses are reduced by a factor of 5 for shields placed closer to the tank (up to 50 mm) and by a factor of 2 to 3 for shields located farther away (up to 300 mm), while the best performance is achieved when the shields are welded directly to the tank [4].

In addition, it is relevant whether the leads of a single phase are shielded or whether a structural arrangement is used in which the leads of multiple phases are brought closer together to achieve cancellation of the multiphase field. In star-connected transformers, there is less flexibility in positioning the high-current leads, whereas in delta-connected transformers, the proximity of the leads can be realised in several ways (between the windings, above the windings, below the windings, etc.). It is important to consider the distance between the leads and the tank, as well as the locations of potential local heating, since it is preferable to arrange the leads in close proximity in the lower part of the tank where the oil is cooler [25]. This measure is particularly important for generator transformers, where

the lead currents can reach several tens of kiloamperes and by applying this measure, tank losses and the need for electromagnetic shielding are significantly reduced [33].

A similar principle is applied in low-magnetic field distribution transformers (with reduced external magnetic field), where the LV leads are divided into two groups of four (N1-U1–V1–W1 and N2-U2–V2–W2) and the leads of each group are positioned close together so that the magnetic fluxes of all three phases cancel out, thereby reducing the external magnetic field of the transformer [38].

5.2. Stray Losses in Cover

The mechanism of stray loss generation in the cover involves the leakage magnetic field from the windings, the magnetic field from the terminals and an additional effect from circulating currents at the junction between the tank flange and the cover (in the case of non-welded covers) [23,24]. In terms of orientation, the leakage field from the windings generates eddy currents in both the cover and the tank in a similar way. However, due to the greater distance between the cover and the windings and the presence of magnetic shields on the tank, the influence of the winding leakage field on cover losses is relatively small compared to its effect on the tank.

What is specific to the cover is that the terminals (with high-current terminals being the most unfavourable case) pass through it and continue into the bushings. When the bushings are installed vertically, the orientation of the leakage magnetic field is radial with respect to the conductor axis, i.e., tangential to the surface of the cover. In this case, the highest losses occur in the immediate vicinity of the bushing opening, with the specific losses in the bushing mounting plates decreasing with the square of the distance [19]. While magnetic shunts are commonly employed to reduce stray losses, their application on the cover plate is not feasible due to its complex geometry [39]. To reduce these losses, inserts made of non-magnetic material are used along the edge of the bushing opening or between the phases, while for the highest current ratings, part or all of the cover is made of non-magnetic material (Figure 8). Practice has shown that this measure is justified for bushing currents exceeding 800 A, where the stray losses, depending on the design of the non-magnetic inserts, are reduced by 30–60% [7,15,23] or even up to almost 80% [39] in the case of 4200 A passing through the cover.

In contrast to direct mounting on the cover, when bushings are mounted on turrets above the cover, high-current terminals can also cause overheating of the turret itself. Therefore, in addition to using non-magnetic materials, electromagnetic shields are installed on the inner wall of the bushing turret. In general, care must be taken when using electromagnetic shields under the cover near non-magnetic inserts, as redistribution of the leakage field due to the operation of the shields may lead to increased losses in the non-magnetic parts of the cover [4].

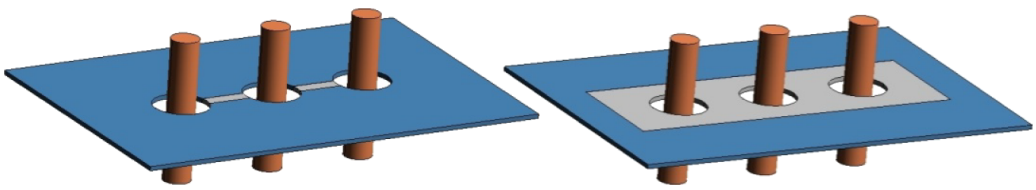


Figure 8. Example of non-magnetic inserts between phases (**left**) and a non-magnetic mounting plate (**right**) on the cover. Source: reproduced with permission from Ref. [23], original author, 2008.

When high-current terminals and bushings are located near the edge of the cover, i.e., close to the tank flange to which the cover is attached, the leakage flux induces circulating currents through the bolts connecting the cover and the tank. For non-welded covers, there is a material discontinuity (a gasket is placed between the cover and the

tank), resulting in a concentration of the magnetic field in the connecting bolts, which drives circulating currents between the tank and the cover [40]. Due to weakened galvanic contact (the bolts may loosen slightly over time as a result of temperature changes and vibration), the contact resistance through which the circulating currents close increases. When the field strength exceeds the critical value of 40 A/cm [24,41], local overheating, degradation of insulation (oil) and contact materials (gasket, paint) can be expected. It is recommended that, in such critical locations, the connecting bolts are bridged, i.e., the tank and the cover are short-circuited (typically using tin-plated copper straps) (Figure 9), thereby providing a highly conductive parallel path for the circulating current and reducing local overheating [24,42].

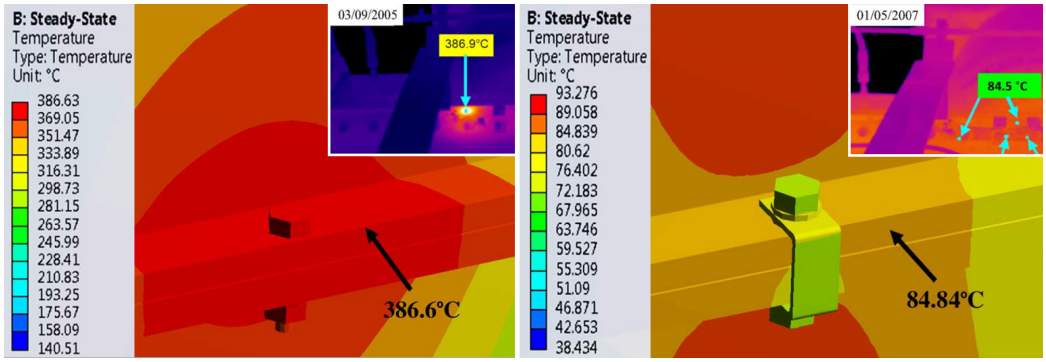


Figure 9. Effect of short-circuiting straps on the temperature (stray losses) of the cover and tank flange. Source: reproduced with permission from Ref. [24], IEEE, 2014.

5.3. Stray Losses in Clamping Frames

By their function, the clamping frames, whose main components are the clamping plates, serve for the radial clamping of the core yoke, while the winding brackets are used for the axial clamping of the windings [23]. The stray losses in the clamping frames arise from three types of magnetic fields to which they are directly or indirectly exposed: the main flux of the core, the leakage flux of the windings and the flux of the leads.

A smaller portion of the clamping frame losses originates from the main flux of the core. As the yoke clamping plates are positioned close to the core yoke, they carry a small part of the main magnetic flux, proportional to the ratio between the relative permeability of the structural steel of the clamping plate and that of the high-permeability laminated core [19]. This principle is explained in more detail in the section on flitch plates.

However, the most significant losses in the clamping frames are caused by the leakage field from the windings, as the clamping frames are located directly above and below the main winding duct. Consequently, part of the leakage flux from the windings returns to the core through the clamping frame. In a typical frame design, the winding brackets are positioned perpendicular to the leakage field of the windings and act as magnetic flux directors, increasing the flux density at the junction between the bracket and the clamping plate, where the flux path closes towards the core and where the clamping plate hot-spot usually occurs [23,43]. Furthermore, in power transformers, high-current leads placed close to the clamping frame often pass over the brackets or supports, which may also create a local hot-spot. Therefore, special attention should be paid to maintaining a sufficient distance between the leads and the clamping frame.

One measure for reducing clamping frame losses caused by the leakage field of the windings is to axially displace the clamping plates and brackets (either together or separately) away from the windings. In the case analysed [44], moving the clamping plate away from the window reduced the losses severalfold, while displacing only the brackets decreased the losses by about 35%. An alternative to increasing the distance of the brackets

is to use a non-magnetic material, which alters the spatial reluctance and redirects the magnetic flux further towards the tank, as non-magnetic brackets present a higher magnetic reluctance along the flux path. By selecting a more expensive non-magnetic material, the need for axial displacement of the brackets is eliminated, achieving the same effect as if magnetic brackets were moved significantly further from the edge of the clamping plate and the leakage field of the windings (Figure 10).

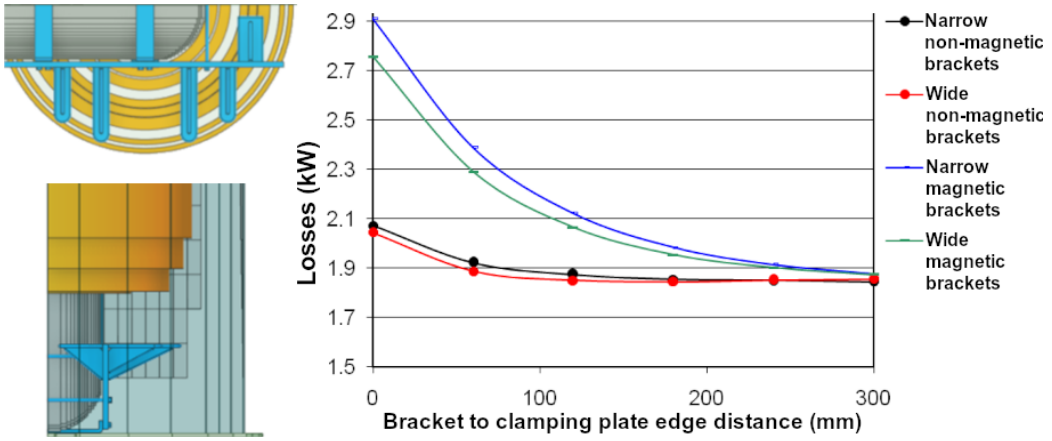


Figure 10. Typical position of brackets in the leakage field of the windings (**left**) and the influence of the axial position and material of the brackets on clamping frame losses (**right**). Source: left image created by the authors; right image adapted with permission from Ref. [23], original author, 2008.

When using non-magnetic material, caution is required because its large penetration depth compared to structural steel (Table 2) allows the field to penetrate deeply into the non-magnetic steel, resulting in losses over a larger volume than in magnetic steel, where losses are confined to a layer only a few millimetres thick [15]. This is particularly important when the non-magnetic material is positioned along the path of a strong leakage flux attracted by the core, as in this case the losses in the non-magnetic steel may exceed those in the magnetic steel [26].

In addition to the axial displacement of the clamping frame from the windings, losses in the clamping frame and other structural components can be reduced by installing three-phase magnetic shunts above and below the windings [33] (Figure 11). In this way, the leakage flux of all three phases is captured, reducing stray losses in the clamping system and, indirectly, tank losses. This enables the use of smaller single-phase magnetic shunts on the tank. When installing magnetic shunts, it is essential that they are positioned sufficiently close to the windings. If they are mounted too far from the windings (as limited by the minimum insulation clearance), they may even increase stray losses in the tank due to changes in the leakage field distribution [45].

Ideally, three-phase magnetic shunts above and below the windings would completely cancel the winding leakage flux, theoretically eliminating the need for magnetic shunts on the tank. In practice, however, space limitations for placing such shunts complicate the design and increase the overall cost of the transformer [26,35]. If the shunts do not have sufficient cross-section, magnetic saturation of the material may occur, resulting in an additional increase in the losses of the shunts.

In the case of a 250 MVA transformer with initially installed magnetic shunts on the tank [6], three-phase magnetic shunts positioned above and below the windings reduced total stray losses for 50%, from 159.4 kW to 79.2 kW. The substantial amount of material required for these shunts also contributes to the increased cost of the transformer. In the case of a 500 MVA transformer [26], a total of 11 tonnes of electrical steel was used for

the three-phase magnetic shunts, resulting in a reduction of stray losses by as much as 43% (107 kW).

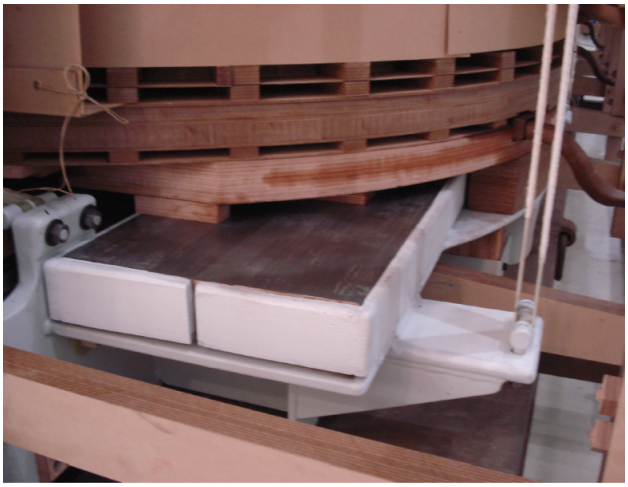


Figure 11. Three-phase magnetic shunts on the clamping frame below the windings of a power transformer. Source: reproduced with permission from Ref. [33], original author, 2024.

In addition to power transformers, this type of magnetic shunts above the windings is also used in low-magnetic field distribution transformers. Its primary purpose is not to reduce stray losses, but to reduce the external magnetic field of distribution transformers. The reduction of clamping frame losses in distribution transformers is intended not to mitigate the leakage field of the windings, but rather to address the effects of high-current LV leads. In Ref. [46], an electromagnetic shield placed between the LV leads and the upper clamping frame is presented, where it was confirmed that the magnetic shunt is more effective (94% loss reduction) than the electromagnetic aluminium shield (56% loss reduction) (Figure 12).

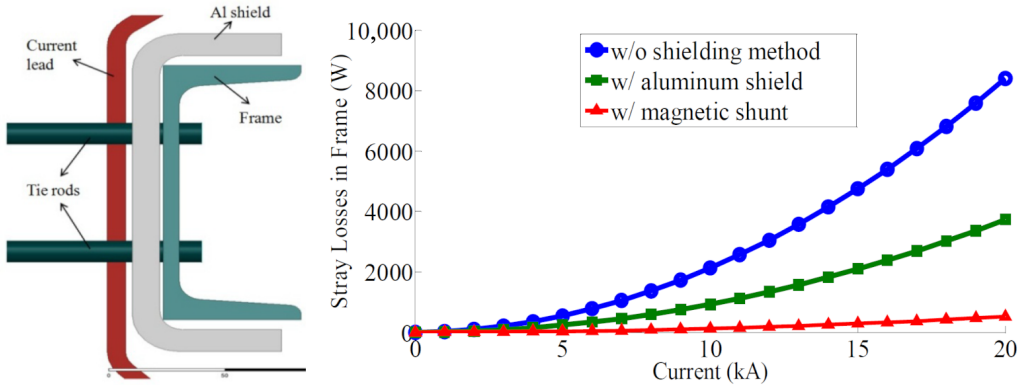


Figure 12. Aluminium shield between the high-current LV leads and the clamping frame (**left**) and stray loss curves in clamping frame with (w/) and without (w/o) shielding methods (**right**) of a distribution transformer. Source: reproduced with permission from Ref. [46], IEEE, 2015.

5.4. Stray Losses in Flitch Plates

Flitch plates are load-bearing structural components that connect the upper and lower clamping systems, ensuring load transfer during lifting of the active part and providing overall core stability during handling in the manufacturing process [23]. They are usually made of structural or non-magnetic steel and, during normal transformer operation, are exposed to two magnetic fields [19]:

- the axial field of the main flux in the core and
- the radial leakage field of the windings.

As the flitch plates are positioned close to the outer limbs of the high-permeability core, they form a parallel path for the magnetic field and therefore carry a small portion of the axial component of the main flux in the core, depending on the ratio between the relative permeabilities of the structural steel of the flitch plates and the laminated core [19]. Although this ratio is very small, at high magnetic flux densities in the core (e.g., 1.7 T), even this small share can cause significant eddy current losses. The use of non-magnetic steel reduces the axial field in the flitch plates by two orders of magnitude (from the order of 0.01 T for magnetic steel to about 0.0001 T for non-magnetic steel), while the current in the non-magnetic steel is further reduced by approximately three to six times due to its higher electrical resistivity compared to magnetic steel.

Unlike the main flux in the core, the leakage magnetic field emerging from the windings is radially incident on the flitch plates and can potentially cause local overheating. One measure to reduce these losses is the axial division of the flitch plates into multiple slots, where slotting can be applied only in the region with the highest leakage flux density or, for higher field intensities (as in generator transformers), a laminated design bonded with epoxy resin is used [5,47] (Figure 13).

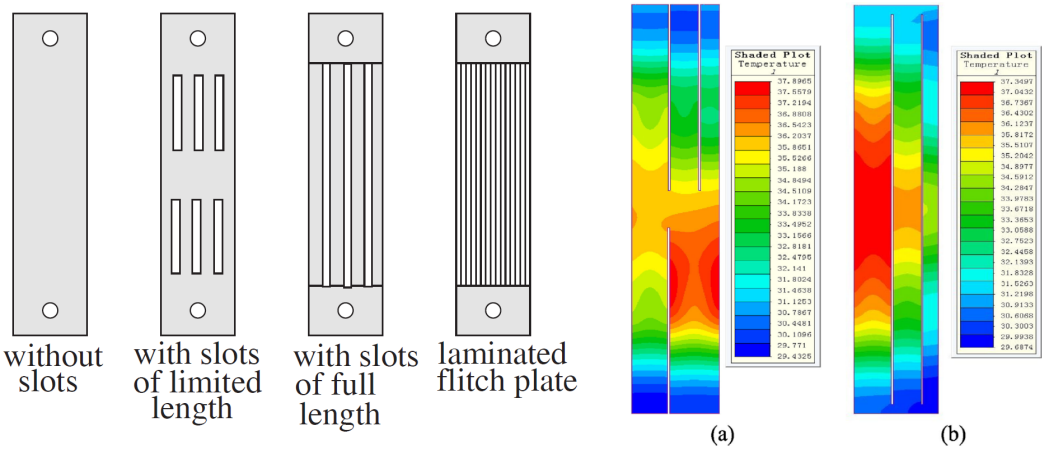


Figure 13. Slotting flitch plates for loss reduction (**left**) and an example of temperature distribution in flitch plates for two thickness designs: (**a**) 8 mm and (**b**) 16 mm (**right**). Source: left image reproduced with permission from Ref. [5], CRC Press, 2013; right image reproduced with permission from Ref. [48], IEEE, 2019.

Regarding the effectiveness of slotting, in theory, the losses in the flitch plate are proportional to the square of its width. Therefore, slotting reduces these losses by a factor equal to the number of slots. Thus, theoretically, dividing a solid plate into four narrower plates reduces the losses by a factor of four. In practice, however, due to the complex behaviour of the radial leakage field in the flitch plates, the actual reduction also depends on the material used.

When magnetic steel is used, due to the smaller penetration depth, surface eddy currents and material saturation occur, causing part of the radial flux to be deflected into the axial direction, which has higher permeability and lower saturation, thus inducing additional losses that are now distributed through the plate thickness [47]. When non-magnetic steel with a larger penetration depth is used, no surface saturation or deflection of the leakage field into the axial direction occurs and therefore, the effectiveness of slotting is higher for non-magnetic material.

However, caution is required when selecting non-magnetic steel, as its losses can exceed those of magnetic structural steel. When non-magnetic steel is used, the component thickness should be kept as small as possible, provided that the mechanical requirements

are satisfied. For flitch plates thicker than approximately 10–13 mm, the losses in non-magnetic steel may surpass those in magnetic steel [5,13,49].

The local losses in the flitch plates are related to the intensity of the incident radial leakage field, which, among other factors, depends on the geometry—namely, the axial height of the windings, the distance between the core and the nearest winding and the width of the main leakage duct [47]. Due to their position in the narrow space between the core and the windings, the flitch plates are relatively shielded from oil flow and heat convection and they are among the structural components most sensitive to rapid temperature rise [50].

Abnormal operating conditions can also be problematic, particularly when a DC component appears in the core field, for example due to geomagnetically induced currents (GICs), which cause half-cycle core saturation, a significant increase in higher harmonics, flux leakage from the core and an increase in stray losses in the structural components, with the flitch plates being among the most affected elements due to their proximity to the magnetic circuit [51].

5.5. Core Edge Losses

Although core edge losses are not classified as stray losses in structural components $P_{stray.sc}$, they are included here to provide a comprehensive analysis of all phenomena associated with stray losses, as they are closely related to losses in the clamping structures. Core edge losses occur when the leakage magnetic field from the windings impinges perpendicularly on the core laminations, inducing eddy currents. The dominant core edge losses arise in the outer core packets [5,52,53], occurring primarily in two regions: the Surface Region and the Edge Region, as illustrated in Figure 14. The Edge Region is located at the edges of the packets, where the effect of eddy currents on the magnetic field penetration is minimal (indicated by the dashed blue outline). The Surface Region is located near the surface of the packets, where eddy currents have a stronger influence on the magnetic field penetration (highlighted by the dashed red outline).

Given the small penetration depth of core laminations, which is on the order of the thickness of a single lamination as shown in Table 2, the leakage field in the outer packets may cause material saturation and the occurrence of higher harmonics. This effect significantly increases the local lamination losses, approximately threefold for the reference case presented in Table 3. Consequently, numerical modelling of lamination saturation provides better agreement between calculated and measured results [3]. Although these losses are relatively small compared with the total transformer losses, their localised nature may lead to hot-spot regions and the formation of fault gases.

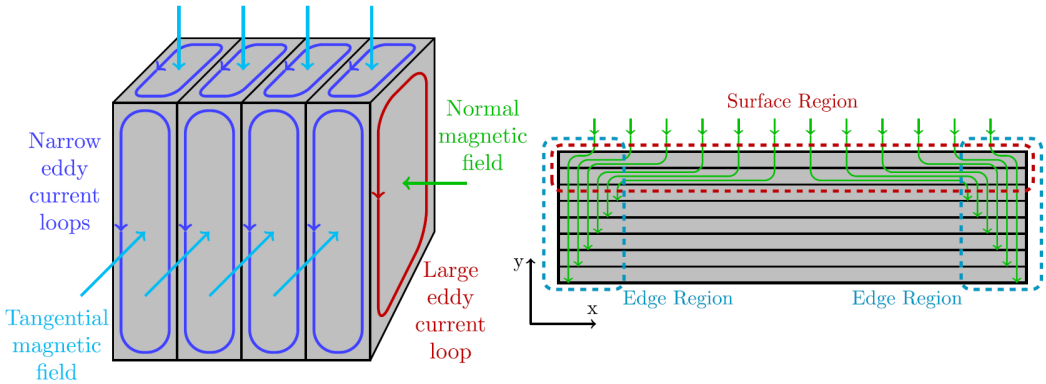


Figure 14. Large and narrow eddy current loops in the laminated steel (**left**) and behaviour of leakage magnetic field and eddy currents in the surface and edge region of the outer core packets (**right**). Source: images reproduced with permission from Ref. [53], original author, 2025.

Considering the anisotropy of electrical steel, the induction of eddy currents caused by the radial leakage field represents a three-dimensional nonlinear problem which, due to the complexity of the geometry, is typically solved using 3-D FEM models. However, such models are time-consuming and impractical for fast estimations. Therefore, the core model is often simplified so that only the first laminations of the outer packets, which account for the highest losses, are modelled in detail, while the remaining part of the core is represented as a homogeneous, non-laminated region [54]. Alternatively, fast hybrid models (2-D FEM models for multiple cross-sections combined with Rabin's method) are used to calculate the magnetic field distribution and the corresponding losses on the surface of the outer core packets [52,53,55].

Core edge losses are also considered in relation to the materials used for clamping structures located near the outer core packets. If non-magnetic materials with greater penetration depth are used for the clamping structures, the radial field passes through them and causes stray losses in the outer core packets. Conversely, when clamping structures made of structural steel with smaller penetration depth are used, a shielding effect is achieved, reducing stray losses in the outer core packets, but resulting in higher losses within the clamping structures themselves. The method for reducing losses in the outer core packets is based on axial segmentation of the laminations in the outer packets, which decreases eddy currents and reduces the severity of hot-spot regions [5].

5.6. Circulating Currents in Structural Components

The occurrence of circulating currents in transformer structural components is a recognized but less thoroughly investigated phenomenon, particularly in the context of the clamping system. While the literature generally addresses circulating currents in structural components under fault conditions, they can also occur during normal operating conditions, representing secondary stray losses.

When multiple earthing points are present between core, clamping system and tank (due to inadequate earthing design, insufficient insulation clearances, metallic debris, or displacement during transport), fault conditions may arise, resulting in circulating currents between the core and/or structural components [56,57]. IEC standard mentions them as one of the causes of thermal faults T2 and T3 [58], as well as circulating currents between the transformer cover and tank induced by the stray field of high-current bushings [24,42].

Circulating currents are also reported in three-phase transformers without a stabilising winding (delta connection), where, under asymmetric operating conditions, the zero-sequence leakage flux closes through the tank and partly through the clamping structure, causing additional losses and circulating currents [5,19,59]. It is important to distinguish between short-term asymmetry (e.g., single-phase short circuit), which generally does not lead to thermal faults in the insulation, and long-term asymmetric loading or resonant earthing of the network, where circulating currents can cause the formation of fault gases and degradation of the transformer insulation.

On the one hand, conventional eddy currents are induced in structural components by the penetration of the magnetic field into the material, while circulating current losses, if present, are superimposed on these eddy current losses. In Ref. [41], excessive losses were reported in the tie bolts of the clamping system (headless bolts threaded at both ends) exposed to the stray magnetic field, along with measures for their reduction, such as electromagnetic shielding using copper or aluminium tubes or the use of non-magnetic materials. However, the additional losses caused by circulating currents that may be closed through these same connecting elements were not considered.

According to the literature, circulating currents arise due to potential differences at the joints of the core and/or between two or more structural components, i.e., equalising

currents between multiple earthing points. This is initially prevented by earthing the core, clamping system and tank at a single point (single-point earthing), as illustrated in Figure 15, thereby avoiding the formation of closed loops between them. The effectiveness of this arrangement is verified by performing the insulation test of the core, clamping structure, and tank [60], which confirms that these components are properly insulated from one another (Figure 16). Improper or degraded earthing is, in fact, one of the most frequent causes of transformer magnetic circuit faults, accounting for approximately 3% of all failures in network transformers with voltage ratings above 100 kV [57].

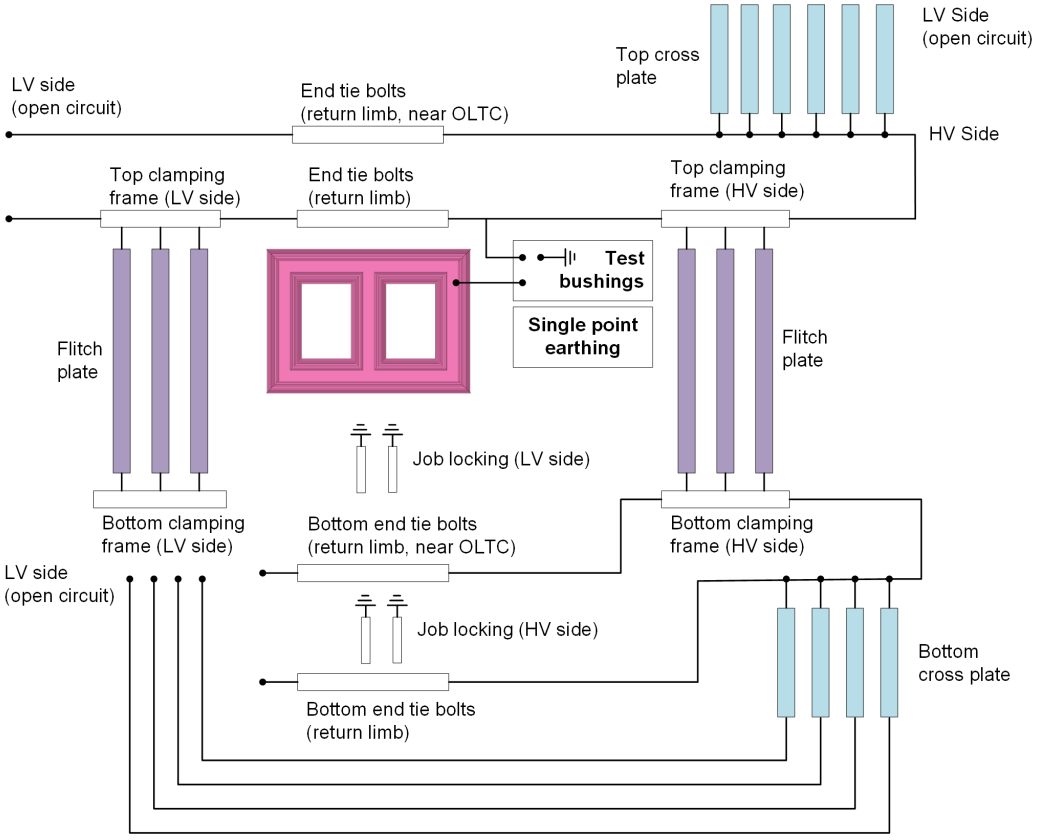


Figure 15. Single-line diagram of the magnetic circuit earthing for the core and clamping system components using the single-point earthing principle. Source: authors, adapted from Ref. [57].

The loss of effective earthing or the presence of multiple earthing points may result from displacement of the active part and mutual short-circuiting of transformer components caused by a short circuit, transportation, damage to insulated tie bolts passing through the yoke, contact between the yoke laminations and the tank bottom, sedimentation, moisture ingress and similar factors.

As previously mentioned, circulating currents are associated not only with fault conditions (e.g., multiple earthing points), but also with normal operating conditions in which closed loops exist within a structural component (e.g., the clamping system), allowing equalising currents to circulate in an attempt to counteract the flux that induces them. Together with conventional local eddy current losses, these circulating currents can cause excessive losses, which may lead to a thermal fault.

In this context, Figure 17 shows the measurement of the hot-spot area within the clamping system (nut, washer, tie bolt), performed during a reduced short-circuit test of the active part (temporary loading of the active part outside the tank at one third of the short-circuit test voltage). The test confirmed the location of fault gas generation and oil carbonisation that had occurred during the routine temperature-rise test. The reduced

short-circuit test of the active part also confirmed the presence of high circulating currents in the tie bolts of the clamping system. All measurements were carried out at the facilities of KONČAR—Distribution and Special Transformers Inc., Zagreb, Croatia.

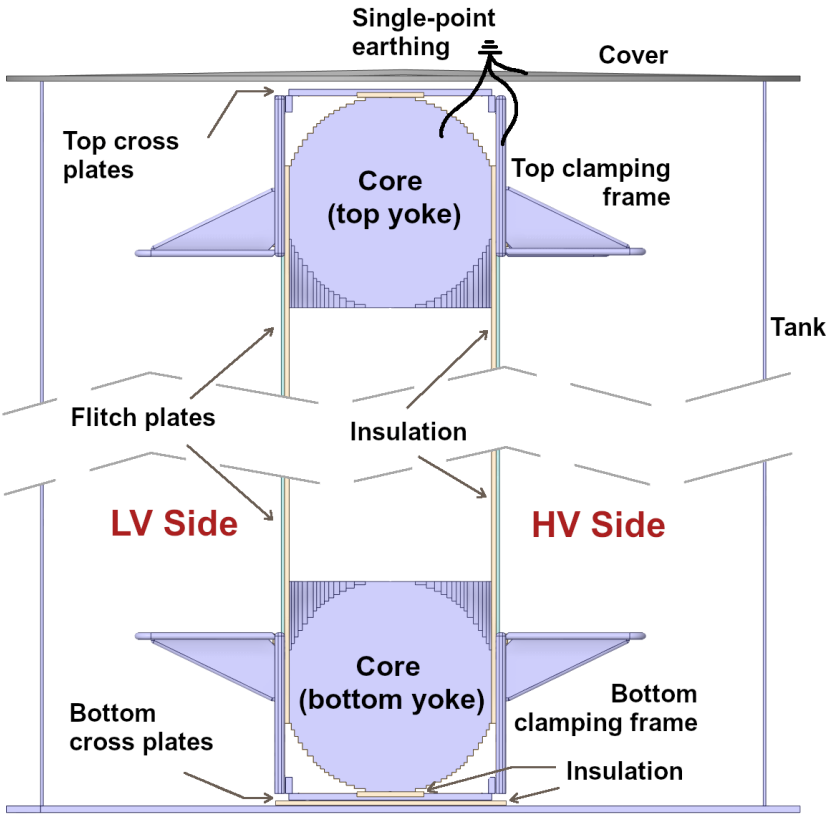


Figure 16. Example of mutual insulation between the core, clamping system and tank. Source: authors, adapted from Ref. [57].

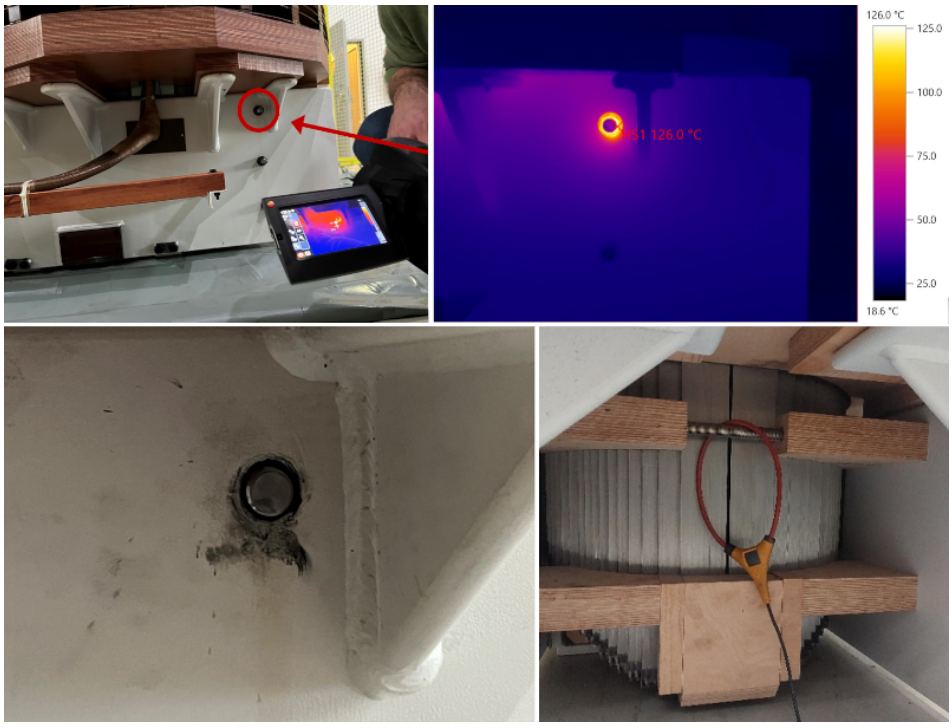


Figure 17. Detection of thermal fault, measurement of hot-spot temperature and circulating currents during the reduced short-circuit test of the active part. Source: authors.

6. Measurement of Stray Losses in Structural Components

On a manufactured transformer, it is almost impossible to directly measure the stray losses by individual components and separate them from the measured load losses [1]. While the ohmic losses $P_{I^2R_{DC}}$ are not frequency-dependent and can be measured separately, the stray losses P_{stray} result from a time-varying magnetic field and are distributed differently among the transformer components.

During transformer load loss measurement, two components are determined: the total load losses P_t and the ohmic losses $P_{I^2R_{DC}}$, while the stray losses P_{stray} are measured indirectly by subtracting the measured values, according to $P_{stray} = P_t - P_{I^2R_{DC}}$. As it is not possible to separate the stray losses by components through measurement (some correspond to stray losses within the windings and some to those outside the windings), they are generally considered together. However, if the windings are made with transposed parallel conductors, the component of stray losses due to circulating currents in the windings can be neglected $P_{stray.cc} \approx 0$, which gives $P_{stray} = P_{stray.we} + P_{stray.sc} + P_{stray.ce}$ [15].

Most power transformers are equipped with on-load voltage regulation, allowing all losses to be measured at three characteristic tap positions (lower, middle and upper). The tap position significantly influences the magnitude of the stray losses [61]. However, it is important to distinguish between the indirect measurement of stray losses during routine transformer testing [60] and the detection of undesirable effects of stray losses during temperature-rise tests [62].

During the temperature-rise test, the transformer is brought to a steady-state thermal operating condition, which requires a certain period, typically several hours. This duration is sufficient for fault gases to develop as a result of P_{stray} and for a thermal fault (thermal degradation of insulation) to be detected. Such effects cannot be observed during routine testing due to the short measurement time.

The temperature-rise test is conducted at the tap position corresponding to the highest current and the highest total load losses, which is usually the lower (minus) tap position that produces the greatest overall heating of the transformer [62]. In contrast, the stray losses in the structural components largely depend on the leakage magnetic field of the windings, which is proportional to the short-circuit voltage, where the inductive component is dominant ($u_k \approx u_\sigma$), serving as a measure of the magnetic field leakage. The higher the value of u_k, the greater the leakage inductance L_σ and the total energy of the leakage magnetic field between the windings W_σ which is primarily responsible for generating $P_{stray.sc}$ [15].

$$W_\sigma = \frac{1}{2\mu}\int_V B_\sigma^2 dV = \frac{1}{2}L_\sigma I^2 \tag{15}$$

While the temperature-rise test is conducted at the lower tap position, the effects of the leakage magnetic field on the structural components are the greatest at the upper tap position (corresponding to the highest u_k). Therefore, there are borderline cases of larger-power transformers with higher u_k values that can pass the temperature-rise test in the lower tap position without thermal failure, whereas such a failure would occur if the test were conducted in the upper tap position (Figure 18).

In the example of a real transformer presented (which has a non-typical high short-circuit voltage for its rated power), the proportion of stray losses P_{stray} in the total load losses P_t varies with the tap position, ranging from 32% to 14%. When considered relative to the rated power of the transformer, the proportion of P_{stray} is at the permillage level, ranging from 1‰ to 0.7‰.

Due to the relatively small proportion of P_{stray} in the total transformer power, the accuracy class of the current and voltage measuring transformers used for the loss measurement is extremely important. The measurement of load losses P_t is performed during the short-

circuit test, where the load is highly inductive (low power factor). Consequently, the load angle is close to 90° (inductive), so any phase angle error of the measuring transformers has a significant impact on the indirect measurement of stray losses.

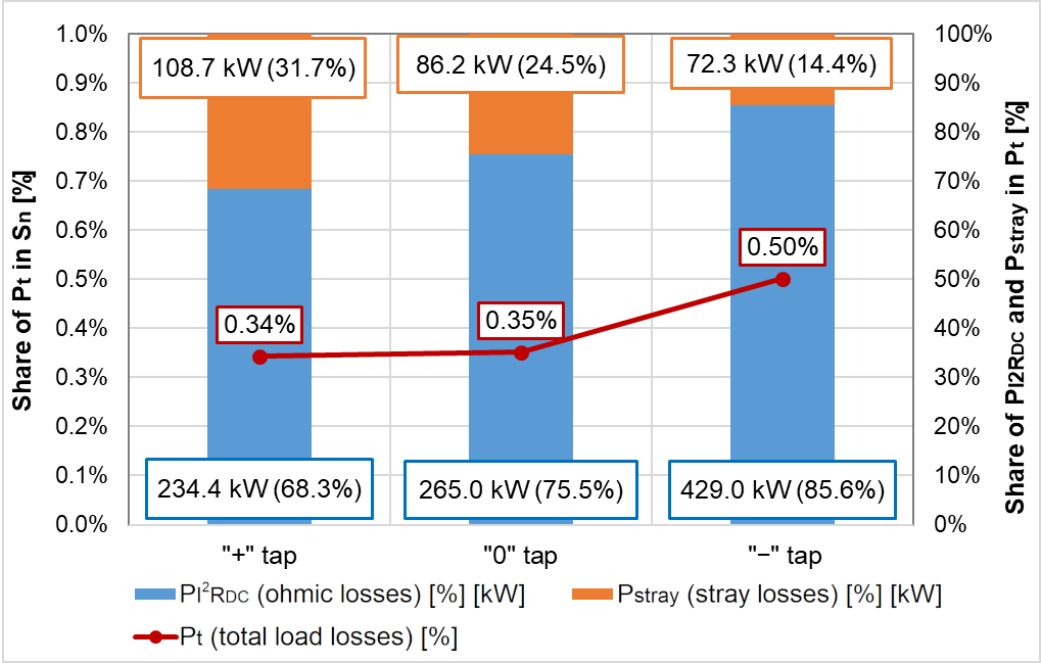


Figure 18. Distribution of measured load losses for three tap positions (S_n = 100 MVA, u_k = 31–36%). Source: authors.

For accuracy class 0.1 (high-precision class used for laboratory measurements and calibrations), the error in measuring the absolute values of voltage and current is 0.1%, while the phase angle error is 5′ (min) [63]. Since a phase angle error of only 1′ (one min) in low power factor measurement results in a loss measurement error of ≈3% [33], in this case the error of the indirect measurement of stray losses P_{stray} is very high—ranging from 10% to 13% for a 1‘ phase error and from 19% to 25% for a 2‘ phase error. This shows that the indirect measurement of P_{stray} inherently includes the uncertainty of the measuring circuit.

Of all stray losses in the structural components $P_{stray.sc}$, for certain transformer configurations, the stray losses in the tank can be measured separately. The distance between the tank wall and the windings significantly affects the distribution of the leakage field, while the angle at which the leakage flux exits the windings determines how much of the leakage flux is directed towards the core and how much towards the tank wall. According to Ref. [64], there is a critical distance T (between the tank wall and the symmetry axis of the main winding duct) at which the influence of the tank becomes negligible (provided $T \geq$ axial height of the winding). Therefore, the stray losses can be measured with and without the tank and in this way, the tank stray losses can be determined indirectly. This applies to tanks equipped with magnetic shunts and/or electromagnetic shields but not to steel tanks without stray loss reduction measures. Another example of separately measuring stray losses in a structural component is provided by dry-type cast resin transformers [65], as they do not have a tank and cover. Therefore, all measured losses refer to the clamping frame and flitch plates.

The method most closely resembling direct measurement of stray losses P_{stray} involves measuring the excitation, specifically the magnitude of the leakage magnetic field (for example, using Hall-effect sensors or measuring coils) at the points where the field enters the structural components [5]. The drawback of this method is its impracticality, as it would

require an array of sensors whose measurements could be used for more accurate analytical and/or numerical loss calculations.

The losses in structural steel can also be determined indirectly through temperature measurements (temperature–time methods), which include two different approaches. In the first method (16), the losses are calculated after the steady-state temperature condition is established, by measuring the temperature difference between the plate (structural element) and the surrounding medium, $\Delta\Theta$. The heat transfer coefficients α [W m^{-2}K^{-1}] are then determined for the structural surfaces A [m^2] through which the heat transfer occurs [5].

$$P_{stray.sc} = \alpha \cdot A \cdot \Delta\Theta \tag{16}$$

The second method (17) considers the rate of temperature change, with the essential condition that the measurement must be performed relatively quickly (within a timescale of seconds) so that the temperature of the observed plate (structural element) remains approximately uniform throughout its volume [66,67]. This method is based on the fact that, for a body initially in thermal equilibrium (e.g., at ambient temperature), its initial rate of temperature rise during sudden heating is proportional to the amount of generated heat—in this case, the eddy current losses [5].

$$P_{stray.sc} = c \cdot \rho \cdot \left(\frac{\partial\Theta}{\partial t}\right)_{t=0} \tag{17}$$

where c is the specific heat capacity [J kg^{-1}K^{-1}], ρ is the material density [kg m^{-3}] and $\left(\frac{\partial\Theta}{\partial t}\right)_{t=0}$ represents the rate of change (gradient) of the plate temperature at the initial part of the measured heating curve.

Equation (17) is valid for plate thicknesses of 5 to 6 mm. An increase in plate thickness leads to a higher rate of convective heat transfer from the hot surface layers to the cooler inner layers of the plate. This effect can be corrected by applying a correction factor that depends on the plate thickness. For example, for a steel ring with a thickness of 8 mm, the error of this method (compared to wattmeter loss measurement) was 5% for the ring in air and 13% for the ring in oil [68].

When performing indirect measurements of stray losses by components, it is important to distinguish between experimental measurements on simple plates—used to validate fundamental physical relationships—and the real operating conditions of transformers with their complex geometries. For this reason, the transformer industry largely relies on numerical multiphysics calculations and the resulting empirical–analytical expressions, which are used for rapid assessments during the design phase. Stray losses in the windings can be calculated with satisfactory accuracy using 2-D numerical models, whereas due to the complex geometry and distribution of the leakage field, accurate calculation of stray losses in the structural components requires the use of 3-D numerical models [4,69].

Electromagnetic–Thermal Coupling and Thermal Fault

Under real operating conditions, the entire stray magnetic flux is coupled with the thermal state of the structural components, which heat up primarily due to eddy currents [70]. The heating is manifested not only by an increase in the total load losses but also by a further rise in oil temperature, higher thermographic readings (where visually accessible), and the presence of dissolved fault gases in the oil resulting from a thermal fault.

Understanding the aforementioned multiphysical (electromagnetic–thermal) coupling, along with knowledge of material properties, geometry and heat transfer coefficients, has become standard practice in the competitive transformer industry [2]. In modelling

electromagnetic–thermal (EM–TH) coupling, the principles of weak and strong coupling are applied [2,70–72], where:

- weak EM–TH coupling represents a linear problem in which the material properties (electrical conductivity, magnetic permeability) and heat transfer coefficients are assumed to be independent of temperature variations.
- strong EM–TH coupling represents a nonlinear problem characterised by temperature-dependent connection between the electromagnetic and thermal calculations.

In strong EM–TH coupling, eddy currents increase the temperature of structural components, which consequently alters their electrical conductivity and magnetic permeability. This, in turn, affects the magnitude of the induced eddy currents, the heat transfer coefficients and ultimately the temperature of the modelled region. This nonlinear problem is solved through successive iterations between the electromagnetic and thermal calculations, which requires significant computational resources, with the computational demands of eddy current analysis usually exceeding those of the thermal calculations [71].

Due to the spatial distribution of eddy currents within the volume of structural components, directly measuring their magnitude is very difficult or nearly impossible. Indirect validation of eddy current calculations and consequently of the EM–TH coupling can be achieved by measuring the temperature of the structural components. In Ref. [73], on a single-phase transformer test model with weak EM–TH coupling, the numerical calculation of the tank hot-spot area was validated by measuring the outer surface temperature of the tank using a thermal camera. The measurement deviation for the test model ranged from 1.3 K to 2.9 K (depending on the winding connection type), while on an actual three-phase 280 MVA transformer, the calculation successfully identified the hot-spot location with a deviation of only 1 °C (the calculated temperature was 102 °C and the measured temperature 103 °C), which is sufficiently accurate for industrial applications (Figure 19).

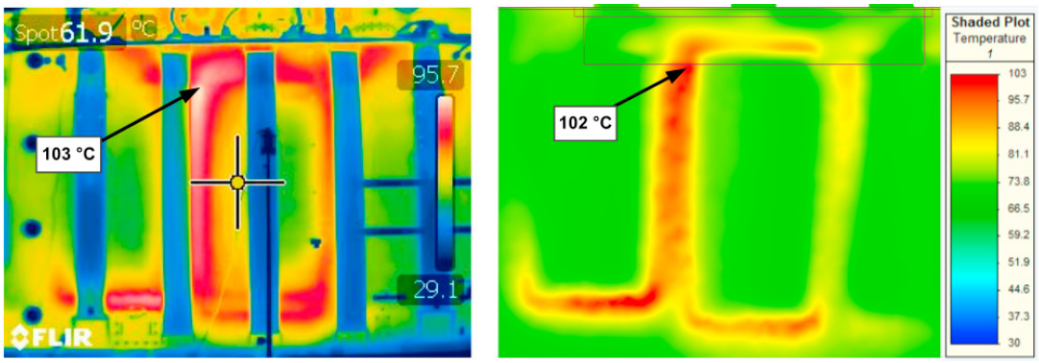


Figure 19. Thermal imaging measurement (**left**) and EM–TH calculation (**right**) of the hot-spot area on the tank shell of a three-phase 280 MVA transformer. Source: reproduced with permission from Ref. [73], original author, 2017.

In addition to thermal imaging for visually accessible parts, the temperature of internal transformer components (e.g., the clamping structure) can be measured using optical-fiber probes of typical accuracy ±1 °C, which is already an established practice for winding hot-spot measurements [72,74]. Example is given in a study [74] where a multiscale electromagnetic–thermal–fluid coupling model was developed for a 50 MVA oil-immersed transformer with a complete cooling circuit. The model's accuracy was validated through a transformer temperature rise test using embedded optical-fiber probes in the winding, with a maximum deviation of 3.1 K.

For the structural components, the same optical-fiber probes were used [43] to measure the hot-spot temperature of the clamping structure at five different positions, and the

deviation between the EM–TH calculation and the measured temperatures was confirmed to be within 1.6 K (Figure 20).

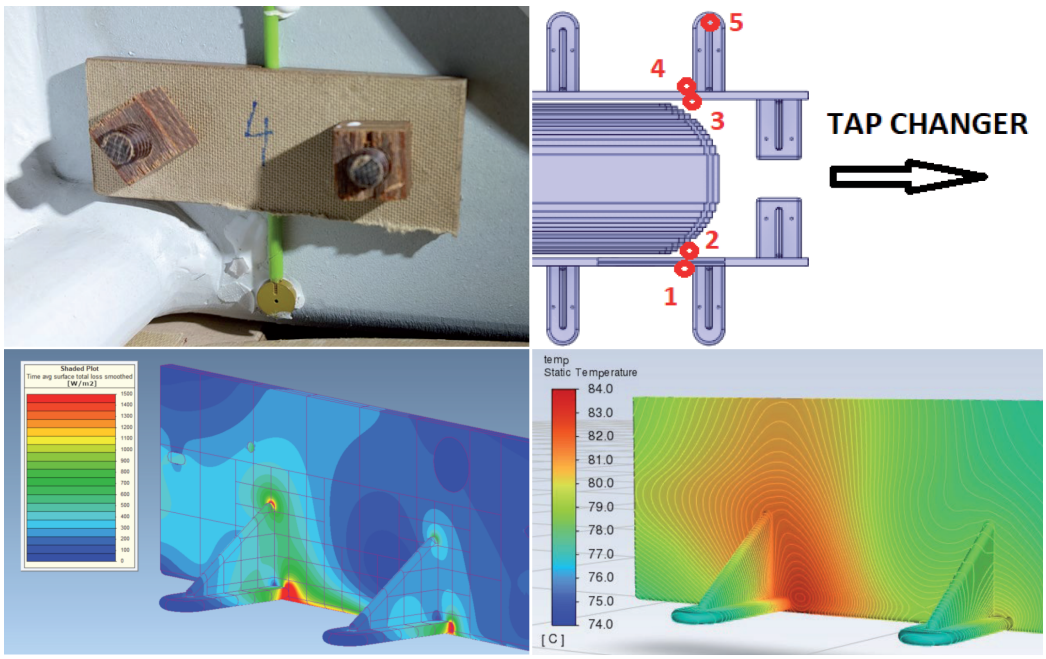


Figure 20. Measurement and calculation of the clamping structure hot-spot area: optical probe mounting (**top left**), positions of all probes on the clamping system (**top right**), electromagnetic calculation (**bottom left**) and thermal calculation (**bottom right**). Source: reproduced with permission from Ref. [43], Journal of Energy, 2024.

Along with direct temperature measurement, the presence of dissolved fault gases in the oil provides an indirect method of temperature assessment. Fault gases indicate a thermal fault, meaning a temperature rise in the insulation above its thermal stability limit. In a properly designed transformer, excessive temperature rise within the insulation system (cellulosic material, paper insulation, oil) results from faults such as partial discharge, electric arcing and local overheating, including stray losses in structural components. The greatest amount of energy is released during an electric arc caused by insulation breakdown, followed by local overheating and then by low-energy partial discharges.

During the thermal degradation of insulation, its molecular structure breaks down, leading to the formation of key fault gases such as hydrogen (H_2), methane (CH_4), ethane (C_2H_6), ethylene (C_2H_4), acetylene (C_2H_2), carbon monoxide (CO) and carbon dioxide (CO_2). These fault gases dissolve in the oil and are detected by dissolved gas analysis (DGA) [58,75], which is considered the best method for assessing the overall condition of a transformer [15]. DGA also enables identification of the type of fault occurring in the transformer. Unlike the mechanisms of fault generation, the interpretation of DGA results is much more complex and typically involves several methods simultaneously. Some methods rely on the proportion of key gases in the sample, while others are based on direct ratios of individual gas concentrations (Doernenburg, Rogers and IEC methods) or indirect ratios represented graphically (Duval triangle and pentagon).

Chromatographic analysis of transformer oil identifies six main types of faults: PD—partial discharges, D1—low-energy discharges, D2—high-energy discharges and three thermal faults, T1, T2 and T3 (Figure 21). For thermal faults, an excessive temperature rise in the insulation may not necessarily result from the fault itself but may also be caused by inadequate cooling, excessive currents in metallic parts in contact with the insulation (such

as poor contact and/or high contact resistance at joints, winding overheating, stray losses in structural components), overloading and similar factors.

Categories of thermal faults, including those caused by excessive stray losses, are defined according to the achieved temperature and visual characteristics as follows [58]:

- T1: thermal fault in oil and/or paper with $\vartheta < 300$ °C and darkening of the paper insulation to a brown colour (e.g., due to excessive stray flux in the frame brackets)
- T2: thermal fault in oil and/or paper with 300 °C $\leq \vartheta < 700$ °C and carbonisation of the paper insulation (e.g., due to poor bolted joints, sliding contacts, cable-to-conductor connections, circulating currents between clamping plates and bolted joints, between clamping structures and core, earthing issues, poor magnetic shield design, etc.)
- T3: thermal fault at temperatures $\vartheta \geq 700$ °C with clear evidence of oil carbonisation, metal discolouration (around 800 °C) or metal melting (around 1000 °C) (e.g., excessive circulating currents in the tank and core, short-circuit loops between core laminations, etc.)

In addition to the six main types of faults, there are also subtypes of faults, of which only those that may result from excessive stray losses are highlighted below:

- S: stray gassing of oil—gas formation at moderate temperatures $\vartheta < 200$ °C due to the chemical instability of mineral oils. Because of modern oil refining techniques, certain oils are more prone to gas formation even at lower temperatures and without the presence of an actual fault (the term stray gassing should not be confused with stray flux, although stray gassing can also be a consequence of stray flux).
- O: overheating of paper or mineral oil at temperatures $\vartheta < 250$ °C (without paper carbonisation and loss of dielectric insulation properties).
- C: possible paper carbonisation.
- T3-H: thermal fault occurring only in mineral oil (without paper involvement).

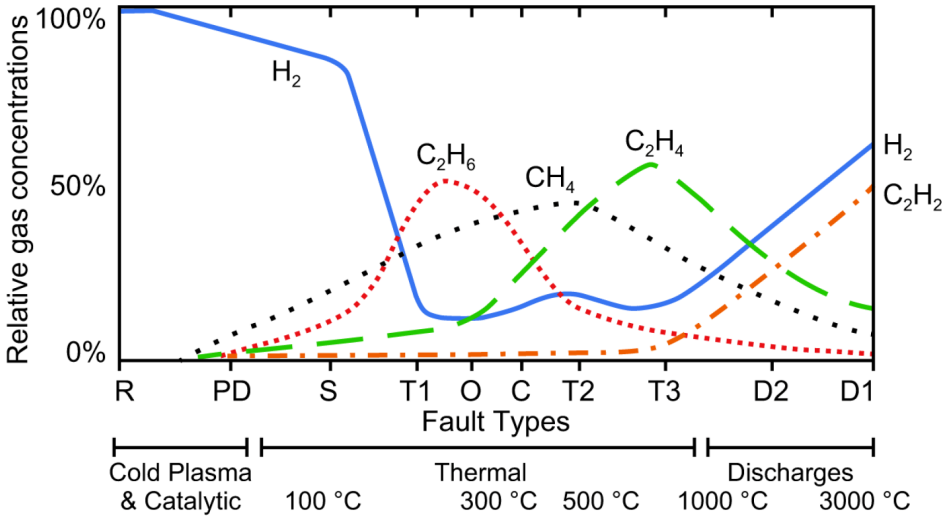


Figure 21. Relative concentration ratio of dissolved fault gases in mineral oil as a function of temperature and fault type. Source: reproduced with permission from Ref. [75], IEEE, 2019.

In thermal faults, the temperature of the hot-spot area is closely related to the temperature class of the insulation materials. Therefore, the same temperature that generates fault gases in conventional insulation materials does not cause gas formation in high-temperature insulation classes. Class A is the most commonly used temperature class for insulation materials, with 105 °C as the maximum permissible temperature. For this class, the material is expected to maintain its relative thermal endurance index for temperatures

between 105 °C and 120 °C [76]. In Class A, the decomposition of cellulosic material (paper) begins at temperatures above 105 °C [58], while mineral oil is considered to start ageing rapidly when it reaches 140 °C [77].

Reaching critical temperatures does not necessarily result in an immediate transformer fault but marks the onset of insulation material degradation and accelerated ageing. There are abnormal network operating conditions (disturbed operation) under which transformer loading above the rated values is permitted [77], provided that the temperature at the metal–insulation interface does not exceed the maximum allowable values (Table 4). Under such transformer overload conditions, the stray losses $P_{stray.sc}$ increase approximately in proportion to the square (or a slightly higher power) of the current (10) and (11).

Table 4. Maximum permissible temperature at the contact between metallic parts and the insulation of an overloaded large power transformer. Source: adapted with permission from Ref. [77], IEC, 2018. (IEC 60076-7 ed. 2.0 "Copyright © 2018 IEC Geneva, Switzerland. www.iec.ch")

Types of Loading	Current [p.u.]	Metal–Cellulose Interface [°C]	Metal–Oil Interface [°C]
Normal cyclic loading	1.3	120	140
Long-time emergency loading ($t >$ week and more)	1.3	140	160
Short-time emergency loading ($t <$ 30 min)	1.5	160	180

7. Conclusions

The conductive structural components of a power transformer, such as the tank, cover, and clamping system, are made of structural steel, which is primarily intended for mechanical functions. Therefore, these components are not intended to carry electrical current. However, the alternating magnetic field induces eddy currents within them, which act to oppose their source. In a transformer, two main sources of eddy current excitation can be identified: the stray magnetic field originating from the windings and the magnetic field generated by current leads.

The stray magnetic field penetrating a conductive material is simultaneously attenuated, so in magnetic steel, eddy currents are usually localised in the surface layer of the component. The main factors influencing the distribution of eddy currents are the ratio between material thickness and penetration depth ($2b/\delta$), as well as the incidence of the alternating magnetic field on the component it penetrates. These two factors together define the relationships and guidelines for selecting different materials (non-magnetic steel, aluminium, copper, electrical steel) to reduce stray losses.

Stray losses represent the smallest share of total load losses in a transformer, yet they increase the fastest with transformer rating, making their effects most pronounced in large-power transformers. A distinction is made between stray losses within the winding (the larger portion) and stray losses outside the winding (the smaller portion), which include losses in structural components.

For each structural element, primary measures can be applied to significantly reduce total stray losses (e.g., magnetic shielding of the tank) and/or secondary measures to eliminate hot-spot areas (e.g., slotting flitch plates). In the latter case, these are localised losses that may not be significant in magnitude but can lead to thermal faults and transformer failure. Even when primary measures are applied, critical hot-spots may still occur because each structural element has its own spatial position and geometric configuration that interacts differently with the tangential and radial components of the stray magnetic field.

All measures to reduce stray losses are essentially aimed at controlling the stray magnetic flux and the magnitude of eddy currents. For tanks, magnetic and electromagnetic

shielding are the most common measures, as well as maintaining adequate magnetic clearance between leads and/or arranging them to counteract the stray magnetic field. Modern transformer tanks are typically equipped with single-phase magnetic shunts (passive shielding), while electromagnetic shields (active shielding) are used to eliminate hot-spot areas.

For the cover, a specific issue arises from high-current terminals passing through openings, where non-magnetic inserts are used to reduce local losses or, in turret-type designs, electromagnetic shielding is applied. In addition, for non-welded covers, the concentration of the stray field in the connecting bolts between the cover and the tank can cause circulating currents, which are eliminated by installing parallel, highly conductive short-circuiting straps.

The frame brackets located in the winding stray field act as magnetic flux directors towards the core, increasing flux density and eddy current intensity at the junction between brackets and clamping plates, thus creating potential hot-spot areas. The main measures to reduce losses in the clamping structures include axially distancing the clamping plates and/or brackets from the winding stray field and/or using non-magnetic steel, bearing in mind that, for greater thicknesses, losses in non-magnetic steel may exceed those in magnetic steel. Additionally, three-phase magnetic shunts may be mounted on the clamping system to capture and cancel out the winding stray flux of all three phases, although this increases structural complexity of the transformer.

Flitch plates are structural components positioned closest to the radial stray flux of the windings. Measures to reduce their local overheating include axial slotting and the use of non-magnetic steel. There is a close relationship between the losses in flitch plates and the core edge losses of the outer core packets, as the use of non-magnetic flitch plates eliminates the shielding effect of the core.

On a manufactured transformer, it is almost impossible to directly measure stray losses by component and separate them from total load losses. Total stray losses are measured indirectly by subtracting the ohmic (frequency-independent) losses from the total load losses. Even with high-accuracy measuring transformers, it is difficult to determine stray losses precisely, as the measurement uncertainty of the phase angle contributes significantly to the total error. Due to the low power factor during the short-circuit test, even a one-minute phase-angle error in the measuring transformers can cause an error of several percent in the measured load losses.

Undesired effects of stray losses, such as thermal faults and fault gases, cannot be detected during routine loss measurements but only during temperature-rise tests, when the transformer reaches steady-state operating temperature, which takes several hours. The temperature-rise test is usually performed at the minimum tap position, where current and total losses are highest, whereas stray losses largely depend on the short-circuit voltage, which is highest at the maximum tap position. Consequently, borderline cases may occur in which local overheating due to stray flux is acceptable at the minimum tap but critical at the maximum tap.

Nevertheless, sufficiently accurate calculation of localised losses can be achieved using coupled electromagnetic-thermal numerical models, which are indirectly validated by measuring hot-spot temperatures using thermal cameras or optical probes. This method has proven accurate enough for industrial application, with deviations of only 1–2 °C, although it still requires considerable computational resources and is not practical for routine use.

The mechanisms of stray-loss generation in transformer structural components and the main mitigation measures are well known in the transformer industry. However, less-studied cases occur in the clamping system, where circulating currents may be su-

perimposed on conventional eddy currents, potentially causing localised overheating of structural parts and the occurrence of thermal faults.

Author Contributions: Conceptualization, S.M.; methodology, S.M.; formal analysis, S.M.; investigation, S.M.; resources, S.M.; data curation, S.M.; writing—original draft preparation, S.M.; writing—review and editing, D.Ž. and S.M.; project administration, D.Ž. All authors have read and agreed to the published version of the manuscript.

Funding: This research received no external funding.

Data Availability Statement: The data presented in this paper are available upon request from the corresponding authors.

Conflicts of Interest: Author Stipe Mikulić was employed by the company KONČAR—Distribution and Special Transformers Inc. The remaining authors declare that the research was conducted in the absence of any commercial or financial relationships that could be construed as a potential conflict of interest.

Nomenclature

The following abbreviations are used in this manuscript:

2-D	Two-dimensional
3-D	Three-dimensional
AC	Alternating current
DC	Direct current
DGA	Dissolved gas analysis
EM–TH	Electromagnetic–thermal
FEM	Finite element method
GIC	Geomagnetically induced current
GOES	Grain-oriented electrical steel
HV	High voltage
IEC	International electrotechnical commission
LV	Low voltage
MM	Magnetic steel
NOES	Non-oriented electrical steel
PD	Partial discharge
RMS	Root mean square
SS	Non-magnetic steel
A	Area (surface)
α	Heat transfer coefficient
b	Half-plate thickness
b_{min}	Minimum half-plate thickness
$\boldsymbol{B}$	Magnetic flux density
B_σ	Leakage magnetic flux denisty
B_m	Maximum magnetic flux density
$\boldsymbol{E}$	Electric field strength
f	Frequency
H	Magnetic field strength
h	Plate height
I	Current
$\boldsymbol{J_e}$	Induced eddy-current density
K_h, K_e, K_a	Coefficients of hysteresis, eddy current, and anomalous (excess) losses
l	Plate width
L_σ	Leakage inductance

μ	Magnetic permeability
μ_0	Magnetic permeability of vacuum
μ_r	Relative magnetic permeability
n	Induction-dependent exponent
∇	Nabla (vector differential operator)
P_0	No-load losees
P_a	Anomalous (excess) losses
P_{aux}	Auxiliary losees
P_e	Eddy-current losses (generated according to Faraday's law of induction)
P_{er}	Eddy-current losses under radial (normal) magnetic excitation
P_{et}	Eddy-current losses under tangential magnetic excitation
$P_{et.thick\ plate}$	Eddy-current losses in a thick plate under tangential magnetic excitation
$P_{et.thin\ plate}$	Eddy-current losses in a thin plate under tangential magnetic excitation
P_h	Hysteresis losses
$P_{I^2R_{DC}}$	DC ohmic (Joule) losses
P_{stray}	Stray losses
$P_{stray.cc}$	Stray losses within the windings due to circulating currents
$P_{stray.ce}$	Stray losses outside the windings in the core (core edge losses)
$P_{stray.sc}$	Stray losses outside the windings in structural components
$P_{stray.we}$	Stray losses within the windings due to eddy currents
P_t	Load losees
$\Phi_{A\sigma}$, $\Phi_{B\sigma}$, $\Phi_{C\sigma}$	Magnetic leakage flux of phase A, B, and C
δ	Penetration depth
γ	Eddy-current parameter $(= (1+j)/\delta)$
c	Specific heat capacity
ρ	Electrical resistivity
σ	Electrical conductivity
S_n	Apparent power
t	Time
u_k	Short-circuit voltage
u_σ	Voltage drop due to leakage reactance
V	Volume
W_σ	Leakage magnetic field energy
X	Ratio of linear dimensions
Θ, ϑ	Temperature
ω	Angular frequency

References

1. Cheng, Z.; Hu, Q.; Takahashi, N.; Forghani, B. Stray-field loss modeling in transformers. In Proceedings of the International Colloquium Transformer Research and Asset Management, Cavtat, Croatia, 9–12 October 2009.
2. Cranganu-Cretu, B.; Kertesz, A.; Smajic, J. Coupled Electromagnetic–Thermal Effects of Stray Flux: Software Solution for Industrial Applications. *IEEE Trans. Ind. Electron.* **2010**, *57*, 14–21. [CrossRef]
3. Bíró, O.; Baumgartner, U.; Koczka, G.; Leber, G.; Wagner, B. Finite element method for nonlinear eddy current problems in power transformers. In Proceedings of the International Colloquium Transformer Research and Asset Management, Dubrovnik, Croatia, 16–18 May 2012.
4. Sitar, R.; Janić, Ž. Impact of electromagnetic shields on local overheating in transformer tank. In Proceedings of the International Colloquium Transformer Research and Asset Management, Dubrovnik, Croatia, 16–18 May 2012.
5. Kulkarni, S.V.; Khaparde, S.A. *Transformer Engineering: Design, Technology, and Diagnostics*, 2nd ed.; CRC Press: Boca Raton, FL, USA, 2013.
6. Taghilou, M.; Mirsalim, M. Strategies for Minimizing Stray Losses in Power Transformers: Effects of Shield Material and Placement. *Electromech. Energy Convers. Syst.* **2025**, *4*, 56–65. [CrossRef]
7. Taghilou, M.; Mirsalim, M.; Eslamian, M.; Teymouri, A. Analyzing the Impact of Cover Design on Stray Losses in High Current Distribution Transformers Based on 3D-FEM Analysis. In Proceedings of the 2024 28th International Electrical Power Distribution Conference (EPDC), Zanjan, Iran, 23–25 April 2024; pp. 1–9. [CrossRef]

8. Stoll, R.L. *The Analysis of Eddy Currents*; Monographs in Electrical and Electronic Engineering; Clarendon Press: Oxford, UK, 1974; pp. xii + 128.
9. Haznadar, Z.; Štih, Ž. *Elektromagnetizam, Elektromagnetska Teorija, Statička i Kvazistatička Polja Svezak 1*; Školska knjiga: Zagreb, Croatia, 1997. (In Croatian)
10. Haznadar, Z.; Štih, Ž. *Elektromagnetizam, Elektromagnetski Valovi i Numeričke Metode Svezak 2*; Školska knjiga: Zagreb, Croatia, 1997. (In Croatian)
11. Betancourt, L.; Martinez, G.; Álvarez, D.; Rosero, J. Losses characterization on distribution transformer windings in frequency domain by means of finite element method (FEM): Part I. In Proceedings of the 4th International Conference on Power Engineering, Energy and Electrical Drives, Istanbul, Turkey, 13–17 May 2013; pp. 103–108. [CrossRef]
12. Betancourt, L.; Martinez, G.; Álvarez, D.; Rosero, J. Losses characterization on distribution transformer windings in frequency domain by mean of finite element method (FEM): Part II. In Proceedings of the 4th International Conference on Power Engineering, Energy and Electrical Drives, Istanbul, Turkey, 13–17 May 2013; pp. 109–114. [CrossRef]
13. Karsai, K.; Kerényi, D.; Kiss, L. *Large Power Transformers*; Elsevier: Amsterdam, The Netherlands, 1987.
14. Prasad, B.; Kulkarni, S.V.; Magdaleno-Adame, S.; Ram, B.S. Analytical Formulation for Eddy Current Losses in Conducting Plates under Normal Magnetic Field Excitation. In Proceedings of the COMPUMAG 2025—25th International Conference on the Computation of Electromagnetic Fields, Naples, Italy, 22–26 June 2025.
15. Žarko, D.; Ćućić, B. *Transformatori u Teoriji i Praksi*; Graphis: Zagreb, Croatia, 2021. (In Croatian)
16. Lotfi, A.; Høidalen, H.K.; Agheb, E.; Nysveen, A. Characterization of Magnetic Losses in the Transformer Tank Steel. *IEEE Trans. Magn.* **2016**, *52*, 6301104. [CrossRef]
17. Bertotti, G. General properties of power losses in soft ferromagnetic materials. *IEEE Trans. Magn.* **1988**, *24*, 621–630. [CrossRef]
18. *EN 10025-2*; Hot Rolled Products of Structural Steels—Part 2: Technical Delivery Conditions for Non-Alloy Structural Steels. European Committee for Standardization (CEN): Bruxelles, Belgium, 2019.
19. Vecchio, R.M.; Poulin, B.; Feghali, P.T.; Shah, D.M.; Ahuja, R. *Transformer Design Principles, with Applications to Core-Form Power Transformers*, 1st ed.; CRC Press: Boca Raton, FL, USA, 2002.
20. Paula, C.; Tomás, G.; Simone, S.; Giuseppe, T. On-site Measurements on Large Power Transformers: Load & no-load losses and PEI. In Proceedings of the 2025 8th International Advanced Research Workshop on Transformers (ARWtr), Baiona, Spain, 13–15 October 2025.
21. *IEC 61378-3:2015*; Converter Transformers—Part 3: Application Guide. International Electrotechnical Commission: Geneva, Switzerland, 2015.
22. Bíró, O.; Baumgartner, U.; Preis, K.; Leber, G. Numerical Modeling of Transformer Losses. In Proceedings of the International Colloquium Transformer Research and Asset Management, Cavtat, Croatia, 12–14 November 2009.
23. Janić, Ž. Unaprjeđenje Konstrukcije Energetskih Transformatora u Cilju Smanjenja Dodatnih Gubitaka. Ph.D. Thesis, University of Zagreb, Faculty of Electrical Engineering and Computing, Zagreb, Croatia, 2008. (In Croatian)
24. Olivares-Galvan, J.C.; Magdaleno-Adame, S.; Escarela-Perez, R.; Ocon-Valdez, R.; Georgilakis, P.S.; Loizos, G. Reduction of Stray Losses in Flange–Bolt Regions of Large Power Transformer Tanks. *IEEE Trans. Ind. Electron.* **2014**, *61*, 4455–4463. [CrossRef]
25. Janić, Ž.; Vlaković, Z.; Šulc, I. Tank loss for different leads arrangement. In Proceedings of the International Colloquium Transformer Research and Asset Management, Cavtat, Croatia, 12–14 November 2009.
26. Štrac, L. Three-Phase Shunts for Stray Magnetic Field. In Proceedings of the International Colloquium Transformer Research and Asset Management, Pula, Croatia, 10–12 May 2017.
27. Magdaleno-Adame, S.; Kefalas, T.D.; Fakhravar, A.; Olivares-Galvan, J.C. Comparative Study of Grain Oriented and Non–Oriented Electrical Steels in Magnetic Shunts of Power Transformers. In Proceedings of the 2018 IEEE International Autumn Meeting on Power, Electronics and Computing (ROPEC), Ixtapa, Mexico, 14–16 November 2018; pp. 1–7. [CrossRef]
28. Chen, Y.; Yang, J.; Yu, H.; Tang, R. Study on eddy current losses and shielding measures in large power transformers. *IEEE Trans. Magn.* **1994**, *30*, 3068–3071. [CrossRef]
29. Selvaraj, S.; Mertens, R.; Caluwaerts, G.; Varrier, M.B.; Mathersa, R. Investigation of impact of magnetic shunt parameters on temperature distribution in transformer tanks. In Proceedings of the International Colloquium Transformer Research and Asset Management, Split, Croatia, 15–17 October 2014.
30. Saleh, A.; Omar, A.; Amin, A.; Adly, A.; Fawzi, T.; El-Debeiky, S. Estimation and minimisation techniques of transformer tank losses. In Proceedings of the Cigré Session 2004, Paris, France, 29 August–3 September 2004.
31. Park, K.H.; Lee, H.J.; Hahn, S.C. Finite-Element Modeling and Experimental Verification of Stray-Loss Reduction in Power Transformer Tank With Wall Shunt. *IEEE Trans. Magn.* **2019**, *55*, 7502104. [CrossRef]
32. Wiak, S.; Welfle, H.; Drzymala, P. Magnetic Field and power losses computation of screen in HV power transformer. In Proceedings of the International Colloquium Transformer Research and Asset Management, Dubrovnik, Croatia, 16–18 May 2012.
33. Valković, Z. *Rasipno Magnetsko Polje i Dodatni Gubici: Predavanje iz Kolegija Transformatori na Poslijediplomskom Doktorskom Studiju*; University of Zagreb, Faculty of Electrical Engineering and Computing: Zagreb, Croatia, 2024. (In Croatian)

34. Moghaddami, M.; Sarwat, A.I.; de Leon, F. Reduction of Stray Loss in Power Transformers Using Horizontal Magnetic Wall Shunts. *IEEE Trans. Magn.* **2017**, *53*, 8100607. [CrossRef]
35. Aleksandar, L. Design of Power Transformers, Lesson 5: Load Losses and Measures to Reduce Additional Losses. Transformers Magazine/Transformers Academy. Available online: https://transformers-magazine.com/transformers-academy (accessed on 10 December 2025).
36. Jain, M.P.; Ray, L.M. Field Pattern and Associated Losses in Aluminum Sheet in Presence of Strip Bus Bars. *IEEE Trans. Power Appar. Syst.* **1970**, *PAS-89*, 1525–1539. [CrossRef]
37. Magdaleno-Adame, S.; Olivares-Galvan, J.C.; Escarela, R.; Raichenko, O.; Kladas, A.G. Hot spots mitigation on tank wall of a power transformer using electromagnetic shields. In Proceedings of the 2014 International Conference on Electrical Machines (ICEM), Berlin, Germany, 2–5 September 2014; pp. 2235–2238. [CrossRef]
38. Rauscher and Stoecklin. Brochure: Distribution Transformers Sustainable and Reliable (Low-Radiation Transformer). 2025. Available online: https://the-rsgroup.com/ (accessed on 10 December 2025).
39. Hashemi, M.H.; Kaplan, K.; Dikmen, S.; Ataei, F. Electromagnetic-thermal evaluation of different non-magnetic material configurations for power transformer tank cover. *Results Eng.* **2025**, *27*, 106352. [CrossRef]
40. Yang, J.; Tang, R.; Wang, C.; Zhou, M.; Chen, Y. New preventive measures against stray field of heavy current carrying conductors. *IEEE Trans. Magn.* **1996**, *32*, 1489–1492. [CrossRef]
41. Turowski, J.; Turowski, M. *Engineering Electrodynamics: Electric Machine, Transformer and Power Equipment Desing*; CRC Press: Boca Raton, FL, USA, 2017.
42. Olivares-Galván, J.C.; Magdaleno-Adame, S.; Escarela-Perez, R.; Ocon-Valdéz, R.; Georgilakis, P.S.; Loizos, G. Experimental validation of a new methodology to reduce hot spots on the screws of power transformer tanks. In Proceedings of the 2012 XXth International Conference on Electrical Machines, Marseille, France, 2–5 September 2012; pp. 2318–2322. [CrossRef]
43. Kovačević, D.; Marković, M.; Blažina, D. Numerical Calculation and Direct Measurement of Local Hot Spot Temperatures in Transformer Clamping Plates. *J. Energy* **2024**, *73*, 8–12. [CrossRef]
44. Janić, Ž.; Valković, Z.; Štih, Ž. Stray Losses in Transformer Clamping Plate. In Proceedings of the ICEM 2006 XVII International Conference on Electrical Machines, Chania, Greece, 2–5 September 2006.
45. Rizzo, M.; Savini, A.; Turowski, J. Influence of flux collectors on stray losses in transformers. *IEEE Trans. Magn.* **2000**, *36*, 1915–1918. [CrossRef]
46. Phani Kumar Mokkapaty, S.; Weiss, J.; Schramm, A.; Magdaleno-Adame, S.; Olivares-Galvan, J.C.; Schwarz, H. 3D Finite Element analysis of magnetic shunts and aluminum shields in clamping frames of distribution transformers. In Proceedings of the 2015 IEEE International Autumn Meeting on Power, Electronics and Computing (ROPEC), Ixtapa, Mexico, 4–6 November 2015; pp. 1–6. [CrossRef]
47. Koppikar, D.; Kulkarni, S.; Srinivas, P.; Khaparde, S.; Jain, R. Evaluation of flitch plate losses in power transformers. *IEEE Trans. Power Deliv.* **1999**, *14*, 996–1001. [CrossRef]
48. Wang, H.; Yang, Q.; Li, Y.; Wang, J.; Zhao, Y. Numerical Calculation and Experimental Verification for Leakage Magnetic Field and Temperature Rise of Transformer Core Tie-Plate. *IEEE Trans. Appl. Supercond.* **2019**, *29*, 0602405. [CrossRef]
49. López-Fernández, X.M.; Ertan, H.B.; Turowski, J. *Transformers: Analysis, Design And Mesurements*; CRC Press: Boca Raton, FL, USA, 2013.
50. Picher, P.; Bolduc, L.; Dutil, A.; Pham, V. Study of the acceptable DC current limit in core-form power transformers. *IEEE Trans. Power Deliv.* **1997**, *12*, 257–265. [CrossRef]
51. Price, P. Geomagnetically induced current effects on transformers. *IEEE Trans. Power Deliv.* **2002**, *17*, 1002–1008. [CrossRef]
52. Jurković, Z.; Jurišić, B.; Župan, T. Fast Hybrid Approach for Calculation of Losses in Outer Packages of Transformer Core Due to Perpendicular Stray Flux. *IEEE Trans. Magn.* **2021**, *57*, 8401504. [CrossRef]
53. Jurkovic, Z.; Trkulja, B.; Petrovic, K.; Jurkovic, M. Quasi-3D Calculation of Stray Losses in Outer Lamination Stack of Power Transformer Core. *IEEE Access* **2025**, *13*, 119279–119291. [CrossRef]
54. Cheng, Z.; Takahashi, N.; Forghani, B.; Gilbert, G.; Zhang, J.; Liu, L.; Fan, Y.; Zhang, X.; Du, Y.; Wang, J.; et al. Analysis and Measurements of Iron Loss and Flux Inside Silicon Steel Laminations. *IEEE Trans. Magn.* **2009**, *45*, 1222–1225. [CrossRef]
55. Jurković, Z.; Jurišić, B.; Župan, T. Multi-Step Approach for Fast Calculation of Magnetic Field in Transformer Tank Shields. In Proceedings of the International Colloquium Transformer Research and Asset Management, Split, Croatia, 29 November–2 December 2023.
56. Yin, Q.; Zhang, Y.; Niu, L.; Gao, N.; Pang, W.; Wang, T. Analysis and Treatment in More Than One Grounding Points on the Clamping Piece of Power Transformer. In Proceedings of the 2020 IEEE 2nd International Conference on Power Data Science (ICPDS), Kunming, China, 12–13 December 2020; pp. 1–5. [CrossRef]
57. Lakhiani, V.K.; Jhala, A.S.; Patel, U.C.; Joshi, Y.V. Magnetic Circuit Circulating Current Issues—Case Study of 167 MVA 400 kV, Single-Phase Auto Transformer (a collaborative analysis by GETCO and T&R). In Proceedings of the 12th IndiaDoble Power Forum, Baroda, India, 1–4 December 2014.

58. *IEC 60599:2022*; Mineral Oil-Filled Electrical Equipment in Service—Guidance on the Interpretation of Dissolved and Free Gases Analysis. International Electrotechnical Commission, Geneva, Switzerland, 2022.
59. Heathcote, M.J. *The J&P Transformer Book: A Practical Technology of the Power Transformer*, 13th ed.; Newnes/Elsevier: Oxford, UK, 2007.
60. *IEC 60076-1:2011*; Power Transformers—Part 1: General. International Electrotechnical Commission, Geneva, Switzerland, 2011.
61. Susnjic, L.; Haznadar, Z.; Valkovic, Z. 3D finite-element determination of stray losses in power transformer. *Electr. Power Syst. Res.* **2008**, *78*, 1814–1818. [CrossRef]
62. *IEC 60076-2:2011*; Power Transformers—Part 2: Temperature Rise for Liquid-Immersed Transformers. International Electrotechnical Commission, Geneva, Switzerland, 2011.
63. Hladek, B. Naponski i Strujni Mjerni Transforamatori. Undergraduate Thesis, Josip Juraj Strossmayer University of Osijek, Faculty of Electrical Engineering, Computer Science and Information Technology, Osijek, Croatia, 2022. (In Croatian)
64. Savini, A.; Turowski, J. Influence of Structure Geometry, Screens and Eddy Currents on the Critical Distance of Tank Wall in Power Transformers. In *Electromagnetic Fields in Electrical Engineering*; Savini, A., Turowski J., Eds.; Plenum Press: New York, NY, USA, 1988; pp. 119–127. [CrossRef]
65. Vurm, V.; Kroták, S.; Svoboda, M.; Knedlík, M.; Rot, D.; Cihla, T. Additional Losses Calculation in Dry-Type Transformer. In Proceedings of the 2025 25th International Scientific Conference on Electric Power Engineering (EPE), Praha, Czech Republic, 27–29 May 2025; pp. 1–6. [CrossRef]
66. Sykulski, J.K. *Computational Magnetics*; Springer: Singapore, 1995. [CrossRef]
67. Kerenyi, D. Stray Load Losses in Yoke-Beams of Transformers. In *Electromagnetic Fields in Electrical Engineering*; Savini, A., Turowski J., Eds.; Plenum Press: New York, NY, USA, 1988; pp. 113–118. [CrossRef]
68. Sitar, R.; Janić, Ž. Application of the temperature-time method for measurement of local power losses in transformer steel parts. In Proceedings of the International Colloquium Transformer Research and Asset Management, Split, Croatia, 15–17 October 2014.
69. Kralj, L.; Miljavec, D. Stray losses in power transformer tank walls and construction parts. In Proceedings of the XIX International Conference on Electrical Machines—ICEM 2010, Rome, Italy, 6–8 September 2010; pp. 1–4. [CrossRef]
70. Cranganu-Cretu, B.; Schneider, M. Coupled electromagentic-thermal analsysis for ABB power transformers. In Proceedings of the International Colloquium Transformer Research and Asset Management, Cavtat, Croatia, 12–14 November 2009.
71. Preis, K.; Bíró, O.; Buchgraber, G.; Ticar, I. Thermal-electromagnetic coupling in the finite-element simulation of power transformers. *IEEE Trans. Magn.* **2006**, *42*, 999–1002. [CrossRef]
72. Ilka, R.; He, J.; Yang, J.; Contreras, J.E.; Cavazos, C.G.; Yin, W. FEA and CFD Based Multi-Physics Modeling, Simulation, and Validation of Oil-Immersed Power Transformers. *IEEE J. Multiscale Multiphys. Comput. Tech.* **2025**, *10*, 304–314. [CrossRef]
73. Sitar, R.; Šulc, I.; Janić, Ž. Prediction of local temperature rise in power transformer tank by FEM. In Proceedings of the International Colloquium Transformer Research and Asset Management, Pula, Croatia, 10–12 May 2017.
74. Peng, M.; Xu, Y.; Hu, Y.; Liu, T.; Wang, Y.; Jiao, R. Multiscale electromagnetic–thermal–fluid field coupling model for oil-immersed transformers. *Front. Mech. Eng.* **2025**, *11*, 1701541. [CrossRef]
75. *IEEE C57.104:2019*; Guide for the Interpretation of Gases Generated in Mineral Oil-Immersed Transformers. IEEE: New York, NY, USA, 2019.
76. *IEC 60085:2007*; Electrical Insulation—Thermal Evaluation and designaton. International Electrotechnical Commission, Geneva, Switzerland, 2007.
77. *IEC 60076-7:2018*; Power Transformers—Part 7: Loading Guide for Oil-Immersed Power Transformers. International Electrotechnical Commission, Geneva, Switzerland, 2018.

Disclaimer/Publisher's Note: The statements, opinions and data contained in all publications are solely those of the individual author(s) and contributor(s) and not of MDPI and/or the editor(s). MDPI and/or the editor(s) disclaim responsibility for any injury to people or property resulting from any ideas, methods, instructions or products referred to in the content.